Mitochondrial Proliferation and Paradoxical Membrane Depolarization during Terminal Differentiation and Apoptosis in a Human Colon Carcinoma Cell Line

Mariangela Mancini,*‡ Benjamin O. Anderson,*‡‖ Elizabeth Caldwell,§ Monireh Sedghinasab,*‡ Philip B. Paty,‖ and David M. Hockenbery‡

*Department of Surgery, University of Washington, Seattle, Washington 98195; ‡Division of Clinical Research and Molecular Medicine, and §Electron Microscope Laboratory, Shared Resources, Administrative Division, Fred Hutchinson Cancer Research Center, Seattle, Washington 98195; and ‖Department of Surgery, Memorial Sloan Kettering Cancer Center, New York 10021

Abstract. Herbimycin A, a tyrosine kinase inhibitor, induces cellular differentiation and delayed apoptosis in Colo-205 cells, a poorly differentiated human colon carcinoma cell line. Cell cycle analysis in conjunction with end labeling of DNA fragments revealed that G_2 arrest preceded apoptotic cell death. Ultrastructural examination of herbimycin-treated cells demonstrated morphologic features of epithelial differentiation, including formation of a microvillar apical membrane and lateral desmosome adhesions. A marked accumulation of mitochondria was also observed. Fluorometric analysis using the mitochondrial probes nonyl-acridine orange and JC-1 confirmed a progressive increase in mitochondrial mass. However these cells also demonstrated a progressive decline in unit mitochondrial transmembrane potential ($\Delta\Psi_m$) as determined by the $\Delta\Psi_m$-sensitive fluorescent probes rhodamine 123 and JC-1 analyzed for red fluorescence. In concert with these mitochondrial changes, Colo-205 cells treated with herbimycin A produced increased levels of reactive oxygen species as evidenced by oxidation of both dichlorodihydrofluorescein diacetate and dihydroethidium. Cell-free assays for apoptosis using rat-liver nuclei and extracts of Colo-205 cells at 24 h showed that apoptotic activity of Colo-205 lysates requires the early action of mitochondria. Morphological and functional mitochondrial changes were observed at early time points, preceding cleavage of poly (ADP-ribose) polymerase.

These results suggest that apoptosis in differentiated Colo-205 cells involves unrestrained mitochondrial proliferation and progressive membrane dysfunction, a novel mechanism in apoptosis.

CELLS in hematopoietic and epithelial lineages maintain tissue homeostasis by a dynamic equilibrium balancing cell proliferation and cell death (91). Cell death in these lineages has been recognized as apoptotic and generally occurs after a terminal differentiation event (17, 126). These physiological cell deaths are remarkably consistent in both timing and location. Mature circulating neutrophils acquire apoptotic morphologies by 30 h after release from the bone marrow (28). Enterocytes undergo apoptosis at villus tips in the small intestine and at the colonic surface after terminal differentiation and transit along the crypt–villus axis (32, 43, 90).

The control of apoptosis after terminal differentiation in these systems is essentially unknown. Although down regulation of expression of bcl-2 and its homologues appears to trigger other instances of physiological apoptosis (43, 66), the patterns of bcl-2 expression in these lineages with rapid cell turnover do not explain the observed patterns of cell death (93). Myeloid expression of bcl-2 is down regulated in metamyelocytes and immature neutrophils (23). Expression of bcl-2 within small and large intestinal epithelia is confined to the lower 1/3 of the crypts (43). Thus, down regulation of bcl-2 significantly precedes apoptotic cell turnover as well as the completion of terminal differentiation. The topographic distributions of the other bcl-2 family members reported to date also do not provide an explanation for the coordinated apoptosis of terminally differentiated cells (8, 55).

Cancer cells often have an immature phenotype representing a block in the normal differentiation pathway (6). Treatments capable of inducing differentiation have been discovered for cancer cell lines in vitro and have in some cases been developed as anticancer therapies (6, 16, 112). In the most successful application of this strategy, all-*trans* retinoic acid induces differentiation of acute promyelocytic leukemias carrying the t(1;19) translocation (22, 26).

Please address all correspondence to Benjamin O. Anderson, Department of Surgery, University of Washington, Box 356410, Seattle, WA 98195. Tel.: (206) 543-6352; Fax: (206) 543-8136.

Complete remissions have been observed with this therapy. Cells that have differentiated in this manner only remain viable for a few days, eventually undergoing apoptosis. Restoration of a normal differentiation program in cancer cells thus appears to also activate an apoptotic mechanism similar to the normal physiological process (83).

Herbimycin A, an antibiotic of actinomycetes origin belonging to the ansamycin group (84), is a natural tyrosine kinase inhibitor that has been reported to induce differentiation in several cell lines, including Rous sarcoma virus-transformed rat kidney cells (76, 118, 119, 122), Rous sarcoma virus-transformed chicken embryo fibroblasts (120), and human K562 myelogenous leukemia cells (45). Recently, we have observed herbimycin A to induce differentiation of Colo-205, a human colon adenocarcinoma cell line derived from malignant ascites, in association with inhibition of constitutive *src* and *lck* tyrosine kinase activities (Paty, P., and N. Rosen, unpublished observations). In the same model, cell death by apoptosis follows differentiation (Mancini, M., and B. Anderson, unpublished observation).

In the present study, we describe striking increases in mitochondrial number within herbimycin-treated Colo-205 cells. Unexpectedly, increased mitochondrial mass did not lead to cellular accumulation of fluorescent probes that reflect mitochondrial transmembrane potential ($\Delta\Psi_m$). These results are consistent with impaired function of newly synthesized mitochondria. Morphologic studies and examination of cell-free assays indicate that progressive, structural changes to mitochondria occur during proliferation and coincide with apoptotic activity in cell lysates.

Materials and Methods

Tissue Culture

The human colon adenocarcinoma cell line Colo-205 was used for all the experiments (108). The cells were maintained in RPMI supplemented with 10% fetal bovine serum (GIBCO BRL, Gaithersburg, MD), 100 U/ml of penicillin, 100 ng/ml streptomycin, and 2 mM L-glutamine, and grown in 75-cm^2 tissue culture flasks at 37°C in a humidified 5% CO_2 atmosphere. They were refed every 48 h and passaged weekly.

Chemicals

Herbimycin A (GIBCO BRL) was dissolved in DMSO at a concentration of 1 mg/ml, stored in 50-μl aliquots at −20°C, protected from light, and thawed immediately before use. *N*-acetyl-L-cysteine (NAC; Sigma Chemical Co., St. Louis, MO) was dissolved in doubly distilled water (100 mM, pH 7.4), stored in aliquots at −20°C, and thawed immediately before use.

Drug Treatment of Colo-205 Cells

Experiments were carried out by subculturing Colo-205 cells at a density of 1×10^5 cells/ml in 10 ml medium/100-mm tissue culture plate. The cells were grown for 24 h before drug treatment. Cells were treated with herbimycin A (300 ng/ml) or vehicle (1% DMSO) and were refed with media containing drug or vehicle at 48-h intervals. Cells were harvested at 0, 24, 48, or 96 h after treatment, collecting both adherent and nonadherent cells. Adherent cells were collected either using 0.02% trypsin with 5 mM EDTA or by gentle scraping with a rubber cell lifter. For the NAC experiments, cells were treated with herbimycin or DMSO, and NAC was added to the cells at time zero at a final concentration of 500 μM.

Transmission Electron Microscopy

Cells were harvested in PBS by gentle scraping and were pelleted by centrifugation. The cell pellets were resuspended in half-strength Karnovsky's fixative for 4–6 h, rinsed in 0.1 M cacodylate buffer, and post-fixed in 1% collidine-buffered osmium tetroxide. Dehydration in graded ethanol and propylene oxide was followed by infiltration and embedding in Epon 812. Approximately 70–90-nm sections were stained using saturated, aqueous uranyl acetate and lead tartrate. Photographs were taken using a transmission electron microscope (100 SX; Jeol, Ltd., Tokyo, Japan) operating at 80 kV.

Detection of Apoptosis

In Situ Labeling of Free 3′-Hydroxyl Ends on DNA. Cells were harvested by gentle scraping, washed in PBS, and counted. An aliquot of 100,000 cells was resuspended in culture media and transferred to a microscope slide by cytospin (800 rpm for 5 min). Cells were fixed in 4% buffered formaldehyde, and fragmented DNA was labeled using a modification of the method of terminal deoxynucleotidyl transferase (TdT)[1]-mediated dUTP-biotin nick end-labeling (TUNEL), described by Gavrieli et al. (32). Briefly, nuclei of cell preparations were permeabilized by incubation with 80 μg/ml proteinase K for 10 min at room temperature. Endogenous peroxidases were inactivated by covering the sections with 2% H_2O_2 for 5 min at room temperature. After incubation for 5 min in TdT buffer (30 mM Tris, pH 7.2, 140 mM Na-cacodylate, 4 mM $MgCl_2$, 0.1 mM DTT), the slides were covered with TdT (0.3 U/μl) and biotinylated dUTP in TdT buffer and incubated for 60 min at 37°C in a humidified chamber (TdT enzyme and dUTP obtained from Boehringer Mannheim, Indianapolis, IN). Negative controls were incubated with biotinylated dUTP in TdT buffer without enzyme. The reaction was terminated by transferring the slides to TB buffer (300 mM NaCl, 30 mM Na citrate) for 15 min at room temperature. The sections were covered with 2% BSA for 10 min at room temperature and immersed in PBS for 5 min followed by incubation with (1:1,000 dilution in PBS) HRP–streptavidin (Zymed Labs., Inc., S. San Francisco, CA) for 30 min at 37°C. The sections were then covered with DAB catalyzed with $NiCl_2$ and H_2O_2 for 10 min and counterstained with 0.25% methyl green in PBS. Positive controls were incubated for 10 min with DNase (100 ng/ml, dissolved in DN buffer: 30 mM Tris-HCl, pH 7.2, 140 mM Na-cacodylate, 4 mM $MgCl_2$, 0.1 mM DTT) before exposure to TdT. After counterstaining, the apoptotic cells were quantified by counting a minimum of 200 cells from at least 5 different random areas of the slide.

Diphenylamine (DPA) Assay for DNA Fragmentation (10). Cells were detached from the plates by scraping and washed in PBS. 5×10^6 cells were resuspended in 500 μl of lysis buffer (5 mM Tris, pH 8, 20 mM EDTA, 0.5% Triton X-100) for 15 min on ice. Lysed cells were then centrifuged at 12,000 rpm in a microcentrifuge for 30 min at 4°C, and the supernatant and pellet were separately analyzed by the DPA assay as previously described (42).

Western Blot Detection of Poly (ADP-ribose) Polymerase (PARP) Cleavage. Cells were harvested by trypsinization and centrifuged at 1,000 rpm for 10 min. 1×10^5 cells were heated for 15 min at 65°C in reducing loading buffer (62.5 mM Tris-HCl, pH 6.8, 6 M urea, 10% glycerol, 2% SDS, 0.003% bromophenol blue, 6% freshly added 2-mercaptoethanol) and loaded on a 6% SDS–polyacrylamide gel. Proteins were then electrotransferred onto a nitrocellulose membrane and analyzed by immunoblotting. The membrane was incubated with Blotto (5% nonfat dry milk, 0.1% Tween 20 in PBS) for 1 h and then overnight with 1:10,000 dilution in blocking buffer of anti-PARP monoclonal antibody (C2-10; Enzyme Bio-Systems, Beloit, WI), followed by 30-min incubation with HRP-conjugated secondary anti–murine IgG (Jackson ImmunoResearch Laboratories, West Grove, PA), diluted 1:2,500 in blotto. The signal was detected using enhanced chemiluminescence (ECL; Amersham Intl., Buckinghamshire, England).

Cell Cycle Analysis

Cell cycle analysis was performed by univariate flow cytometry using either nuclei or whole cell preparations. For nuclei, asynchronously growing cells were harvested without trypsinization in PBS supplemented with 1% FCS, washed, and resuspended at a concentration of 1×10^6 cells in 1.5 ml of ice-cold PBS. After centrifugation, supernatants were discarded, and the cell pellets were resuspended in 250 μl of Buffer A (10 mM Tris-HCl,

1. *Abbreviations used in this paper*: $\Delta\Psi_m$, mitochondrial membrane potential; DHE, dihydroethidium; H_2-DCF-DA, dichlorodihydrofluorescein; NAO, nonyl-acridine orange; PARP, poly (ADP-ribose) polymerase; ROS, reactive oxygen species; TdT, terminal deoxynucleotidyl transferase.

pH 7.5, 20 mM NaCl, 20 mM $MgCl_2$) and incubated on ice for 5 min. 250 μl of Buffer B (Buffer A plus 1% NP-40) were then added to the cell suspension for 5 min on ice. After adding 10 μg/ml of DNase-free RNase, nuclei were incubated at 37°C for 30 min. DNA staining was obtained with 500 μl of propidium iodide solution (PI; Molecular Probes, Eugene, OR) in PBS (100 μg/ml PI, 0.1% Triton X-100, 1% FCS) for 1 h at 4°C in the dark, followed by flow analysis. Whole viable cells were also used for cell cycle analysis and stained with Hoechst 33342 (Sigma Chemical Co.). Cells were incubated in culture with 0.5 μg/ml of Hoechst 33342 for 90 min at 37°C and then harvested by trypsinization and used for flow analysis. To obtain better preservation of cytosolic DNA in apoptotic cells, whole cells were analyzed after fixation with 1% paraformaldehyde (pH 7.4) for 15 min on ice, followed by 70% ethanol. After being washed twice with PBS, the cells were stained with PI according to the protocol described below, and analyzed by flow cytometry. The DNA fluorescence was measured using a FACScan® (Becton Dickinson, Bedford, MA) for PI or FACS® Vantage for Hoechst staining. Data acquisition was performed using the Cell Quest software (Becton Dickinson) and data analysis using the Phoenix Flow System Multicycle AV software.

Assessing Relationship between Apoptosis and Cell Cycle. At each time point, the cells were harvested by trypsinization, washed in PBS, and fixed in 1% formaldehyde (pH 7.4) for 15 min on ice. At the end of the formaldehyde fixation the cells were washed twice in PBS, forcibly pipetted into 5 ml of 70% ethanol, and stored at −20°C until ready for use. On the day of the experiment, the cells were washed twice in PBS and resuspended in 50 μl of TdT reaction buffer containing 10 μl of 5× concentrated buffer solution (1 M sodium cacodylate, 125 mM Tris-HCl, pH 6.6, 1.16 mg/ml BSA), 5 μl of 25 mM cobalt chloride, 12.5 U of TdT enzyme, 0.25 nmoles of fluorescein-dUTP (TdT enzyme and fluorescein-dUTP were both obtained from Boehringer Mannheim), and doubly distilled water up to 50 μl (34, 64). The cells were incubated in this solution for 60 min at 37°C and then rinsed twice with 1.5 ml of 15 mM EDTA, pH 8, and once with 1 ml of 0.1% Triton X-100 in PBS. At the end of the washing, DNA counterstaining was carried out by resuspending the cellular pellets in 1 ml of PI solution in PBS (2.5 μg/ml PI, 10 μg/ml DNase-free RNase) and incubating them for 30 min at room temperature, shielded from light.

Assessment of Mitochondrial Changes

Relative mitochondrial mass was measured by flow cytometry using 10-*n*-nonyl–acridine orange (NAO; Molecular Probes; 67, 88) or 5,5′,6,6′-tetrachloro-1,1,3,3′- tetraethylbenzimidazolcarbocyanine iodide (JC-1; Molecular Probes; 94, 111), analyzed for green fluorescence. Mitochondrial function was indirectly assessed by variation in mitochondrial transmembrane potential measured by rhodamine 123 (14, 49) and JC-1 red fluorescence. ROS production was assessed by oxidation of 2′,7′-dichlorodihydrofluorescein diacetate (H_2–DCF-DA; Molecular Probes) and dihydroethidium (DHE; Molecular Probes) to fluorescent products 2′,7′-dichlorofluorescein (DCF) and ethidium (Eth), as measured by flow cytometry (5, 44, 99, 127).

NAO Staining. Cells were trypsinized, resuspended in 0.5 ml of PBS, fixed in 70% ethanol, and stored until use at −20°C. On the day of each experiment, ethanol was removed by centrifugation, and 1×10^6 cells were washed in PBS and stained with 10 μM NAO in 1 ml of PBS. After incubating for 10 min at room temperature in the dark, cells were washed in PBS and submitted for flow analysis.

Rhodamine 123 Staining. Cells were trypsinized, resuspended in medium at a concentration of 1×10^6/ml, incubated for 30 min at 37°C with 0.5 μg/ml of rhodamine 123, and submitted immediately for flow analysis.

JC-1 Staining. 1×10^6 cells were resuspended after trypsinization in 1 ml of medium and incubated with 10 μg/ml of JC-1 for 10 min at 37°C before flow analysis. Both red and green fluorescence emissions were analyzed after JC-1 staining.

H_2–DCF-DA and DHE Staining. Cells were incubated with 5 μM H_2–DCF-DA or DHE in tissue culture medium for 45 min at 37°C and then washed, resuspended as 1×10^6/ml in PBS, and submitted to flow analysis.

Flow Cytometric Analysis. A FACScan® (Becton Dickinson, Bedford, MA) was used for all the experiments. Forward and side scatters were used to establish size gates and exclude cellular debris and apoptotic cells from the analysis (13, 20). For each experiment both herbimycin- and DMSO-treated cells were analyzed. The excitation wavelength was 488 nm. The observation wavelengths were 530 nm for green fluorescence and 585 nm for red fluorescence. Relative change in mean fluorescence was calculated as the ratio of mean fluorescence channels for herbimycin to DMSO-treated samples.

Cell-free Assay for Apoptosis

Cells were harvested by trypsinization at 0, 24, and 48 h after herbimycin exposure. 5×10^6 cells were rinsed in PBS, and the pellets were resuspended in 300 μl of lysis buffer (20 mM Hepes-KOH, pH 7.5, 10 mM KCl, 1.5 mM $MgCl_2$, 1 mM sodium EDTA, 1 mM sodium EGTA, 1 mM DTT, 0.1 mM PMSF, supplemented with 2 μg/ml aprotinin, 5 μg/ml pepstatin A, 10 μg/ml leupeptin). The samples were left on ice for 15 min and then lysed by 23 strokes with the B pestle in a Dounce homogenizer (Kontes Glass Co., Vineland, NJ), and centrifuged at 1,000 *g* for 10 min at 4°C. The resulting pellet (nuclear fraction) was discarded, and the supernatant (cytosolic fraction) was split in two parts and used for the in vitro apoptosis assay. Protein content of the cell extract was determined by the Lowry method. The lysates were adjusted to a fixed protein concentration (5 μg/μl). Half of each lysate was further centrifuged at 10,000 *g* for 30 min at 4°C. The resulting supernatant (S10 fraction) was collected. A preparation of rat liver nuclei containing 200,000 nuclei/μl of buffer A (10 mM Pipes, pH 7.4, 80 mM KCl, 20 mM NaCl, 5 mM sodium EGTA, 250 mM sucrose, 1 mM DTT) was kindly provided by Michael Wright (University of Washington, Seattle, WA). The cell-free reactions were set up in Eppendorf tubes containing 1 μl of nuclear preparation (200,000 nuclei) and 30 μl of Colo-205 lysate (whole cytosolic fraction or S10 fraction), corresponding to 150 μg of protein. The total volume was adjusted in each tube to 50 μl using dilution buffer (10 mM Hepes, 50 mM NaCl, 2 mM $MgCl_2$, 5 mM EGTA, 1 mM DTT). The samples were incubated for up to 2 h at 37°C and then an aliquot of each reaction (10 μl) was mixed 1:1 with staining solution (200 mM sucrose, 5 mM $MgCl_2$, 80 mM KCl, 15 mM NaCl, 5 mM EDTA, 150 mM Pipes-NaOH, pH 7.4, 10 μg/ml Hoechst 33258, 3.7% paraformaldehyde) and observed for nuclear morphological changes by fluorescence microscopy.

Statistics

Data are reported as mean ±SD except where indicated. Experiments were performed in triplicate. Comparisons among multiple groups were made by a one-way analysis of variance (ANOVA) followed by Fisher's protected least significant difference post-hoc test. 95% confidence limits ($P \leq 0.05$) were considered significant.

Results

Herbimycin A Induces Growth Arrest Followed by Cell Death in Colo-205 Cells

Colo-205 cells treated with herbimycin A in a dose range of 200–500 ng/ml demonstrate growth arrest, evident by 24 h after treatment. A dose of 300 ng/ml produces maximal growth arrest and differentiation, along with maximal inhibition of *src* and *lck* tyrosine kinase activities in Colo-205 cells (Paty, P., and N. Rosen, unpublished observations). Cell count, representing the net result of cell proliferation and cell death, is decreased at 24 h in herbimycin-treated cells compared to cells treated with DMSO alone (Fig. 1 *a*). Loss of cell viability, as measured by trypan blue exclusion, is not apparent in herbimycin-treated cells until 48 h (Fig. 1 *b*), suggesting that the early decrease in cell count in herbimycin-treated cells results primarily from decreased proliferation rather than accelerated death. This finding is confirmed by cell cycle analysis which shows that herbimycin causes fewer cells to be in S phase at 24 h in comparison to control, accompanied by accumulation of the cells in G_2/M at 24–48 h (see Fig. 6 and text below). Both cell count and cell viability continue to decrease throughout the 96-h observation period (Fig. 1, *a* and *b*).

Herbimycin A-induced Epithelial Differentiation Is Associated with Mitochondrial Proliferation

Colo-205 cells appear as small, round cells with scattered spindle-shaped cells by light microscopy. These cells grow

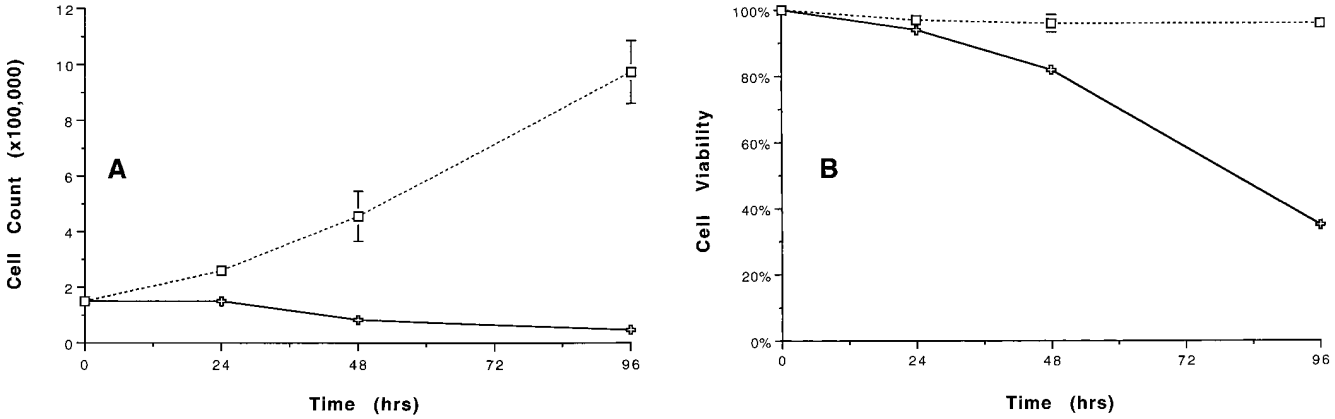

Figure 1. Growth and viability curves of Colo-205 cells treated with herbimycin A, 300 ng/ml (*solid line*), or DMSO vehicle, 1% (*dotted line*). Cell growth, as expressed by number of viable cells/ml media (*A*) and cell viability, as measured by trypan blue exclusion (*B*), progressively decrease in cells treated with herbimycin A. Growth arrest starts 24 h before the decrease in viability becomes evident, suggesting that herbimycin decreases cell proliferation and then induces cell death.

as semi-adherent cells in plastic tissue culture flasks. Addition of herbimycin A triggers a sequence of major morphological changes in Colo-205 cells. At 24 h the cells are adherent and appear larger, flattened, and less rounded. They form aggregates and epithelioid colonies, which become progressively larger from 24 to 96 h (Fig. 2).

Transmission electron microscopy demonstrates the ultrastructural characteristics of Colo-205 cells. Before her-

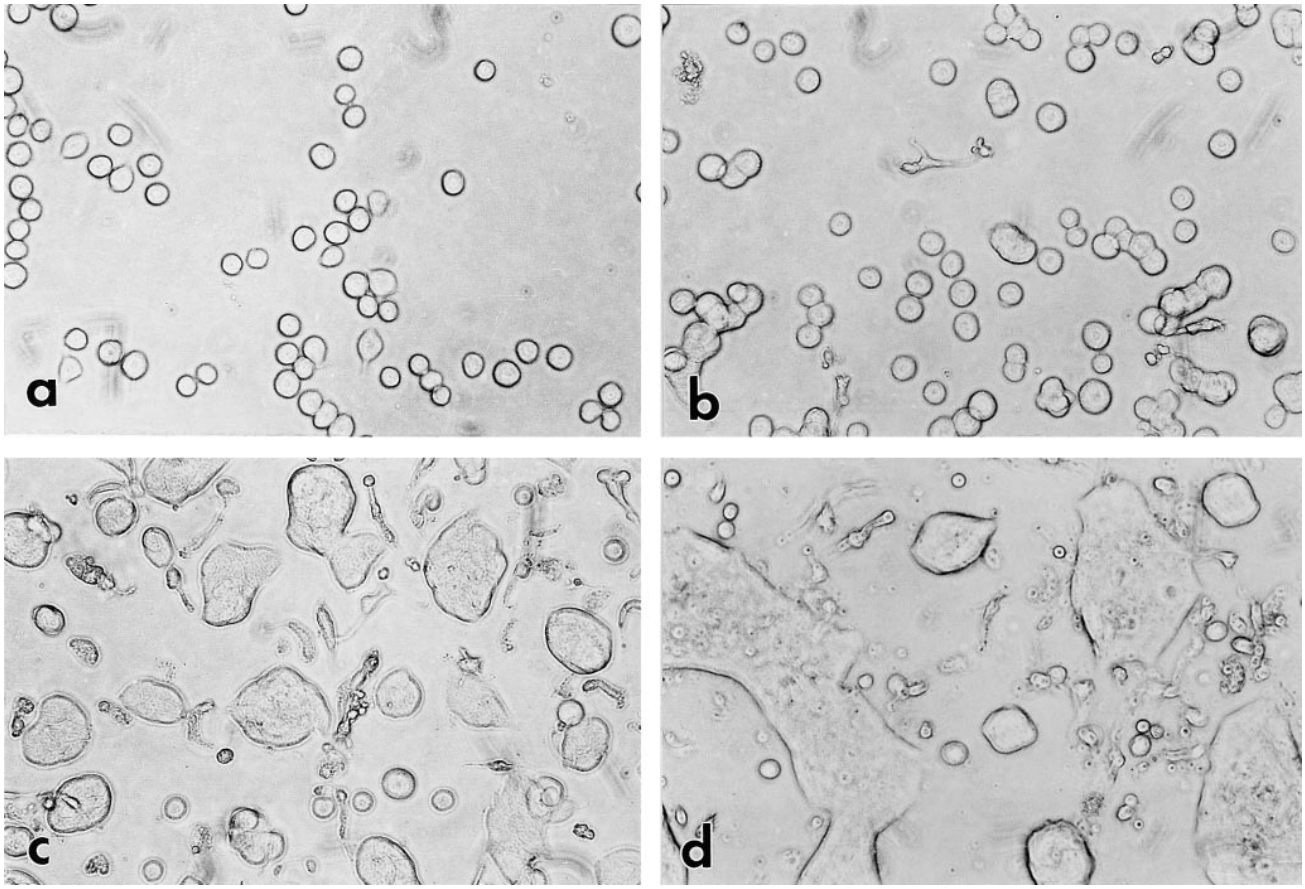

Figure 2. Phase contrast light microscopy images of Colo-205 cells during culture with herbimycin A (300 ng/ml). The small, round Colo-205 cells visible at time 0 (*a*) show increase in size and tendency to form cellular aggregates at 24 h. At 48 h (*c*), the cells appear organized in epithelioid colonies, which appear larger at 96 h (*d*). Dead cells and cellular debris can be observed in culture at 48 and 96 h of herbimycin exposure.

bimycin exposure, they appear as isolated, small, rounded cells, with a high nucleus-to-cytoplasm ratio and a simple cytoplasmic organization with a paucity of organelles (Fig. 3 *a*). By 24 h after herbimycin treatment, Colo-205 cells begin to acquire ultrastructural features of differentiation (Fig. 3 *b*). They appear larger and form a rudimentary polarized monolayer with an emerging brush border. There is a general increase in free ribosomes and rough endoplasmic reticulum. Some cells at 24 h were noted to have increased numbers of mitochondria, many of which are electron dense and have reduced volume as compared to control cells (Fig. 3 *b*).

The differentiated phenotype of Colo-205 cells has progressed by 48 h of herbimycin treatment, when the cells assume a more mature enterocytic morphology that resembles that of the columnar absorptive lineage (77). In particular, the cells acquire a polygonal shape, and cell polarity and the apical brush border are better defined, with well-formed desmosomes connecting adjacent cells close to their apical surface (Fig. 3 *c*). The number and condensation of mitochondria appear further increased at this time point.

At 96 h, surviving cells are found at the free surface of larger cellular aggregates and appear highly differentiated with long, narrow, and more numerous apical microvilli, while underlying cells are apoptotic or appear to be undergoing secondary necrosis (see below). The superficial cells of these clusters have condensed cytoplasm and decreased intercellular contacts as compared to cells after 48 h of treatment (Fig. 3 *d*). Zones of detachment between adjacent cells resemble those observed in terminally differentiated enterocytes of normal colonic mucosa (90). Surprisingly, after 96 h of herbimycin exposure, viable cells show still higher numbers of highly condensed small mitochondria, localized primarily to the apical side of cells (Fig. 3 *d*).

Apoptosis Follows Herbimycin-induced Epithelial Differentiation

Between 48 and 96 h after herbimycin exposure, light microscopy showed a progressive reduction in cellular density, and both intact dead cells and cellular debris were visible (Fig. 2).

As the differentiation process continues, apoptotic figures become increasingly visible by electron microscopy. While barely detectable at 24 h (8/400 cells), intact apoptotic cells (Fig. 4 *a*) and apoptotic bodies (Fig. 4 *b*) are readily apparent from 48 to 96 h. Apoptotic cells demonstrate intact cell membranes with cytoplasmic and chromatin condensation (Fig. 4 *a*). Apoptotic bodies contained either highly condensed chromatin typical of apoptosis or finely dispersed chromatin, resembling a chromatolytic morphology. These latter changes were consistent with post-apoptotic or secondary necrosis (68).

The presence of delayed apoptosis was confirmed by other assays. Tunel, a specific, histologic method for detection of nuclear DNA fragmentation (32), identified 15% of nuclei as apoptotic 48 h after herbimycin addition to the cells (Fig. 4 *c*). The DPA assay, a quantitative measure of soluble DNA released from apoptotic nuclei into the cytoplasm (10), demonstrated DNA fragmentation at 48 and 96 h (Table I). Similarly, DNA histograms of PI-stained Colo-205 nuclei showed a progressive increase in events with sub-diploid DNA content (the "sub-G_1 peak") which is characteristic of apoptosis (82). The frequency of sub-G_1 events was 0, 3, 15, and 42% at 0, 24, 48, and 96 h, respectively (Fig. 5).

These results permit us to identify a sequence of herbimycin-induced events in Colo-205 cells. Growth arrest and differentiation are observed by 24 h. At 48 h, cellular viability begins to decrease, and apoptosis, quantified by Tunel, DPA, and frequency of sub-G_1 events, is detectable. At 96 h the general viability is further reduced and apoptosis increased. Thus, growth arrest, differentiation, and apoptosis proceed sequentially in this model. Mitochondrial number increases progressively at each stage, starting at 24 h. During the program of terminal differentiation of normal colonic mucosa, cell cycle arrest in G_1 precedes differentiation and apoptosis (27). To determine the effect of herbimycin on cell cycle progression, cell cycle analysis of Colo-205 cells was performed.

Cell Cycle Events: G_2/M Accumulation and Its Relationship to Herbimycin-induced Apoptosis

Cell cycle distribution in Colo-205 cells after exposure to herbimycin was assessed by flow cytometric measurement of cellular DNA content. Analysis was carried out first on isolated nuclei stained with PI. In this case cell cycle analysis showed reduction of S phase at 24 h and subsequently, appearance of a progressively larger sub-G_1 population (sub-G_1 peak), indicative of apoptosis (Fig. 6, *top row*).

A different result was obtained when flow analysis was performed on whole cells, either viable and stained with Hoechst 33342 or fixed (1% paraformaldehyde and 70% ethanol) and stained with PI (18). A better preservation of the degraded, low molecular weight DNA inside the apoptotic cells can be achieved in this way (20, 21). Cell cycle analysis of whole cells showed early reduction of S phase at 24 h, as already seen by analyzing nuclei. At 24–48 h, however, an accumulation of cells in G_2/M is evident (Fig. 6, *middle* and *bottom rows*). Careful analysis of the raw data showed a wide shoulder of events at the left of the G_2/M peak at 48 h, suggesting a concealed sub-G_2 peak (Fig. 6, *middle* and *bottom rows*). Indeed, a population of cells with a DNA content below the normal G_2/M content can be detected. Because of its shape and also the observed early decrease in S phase, this peak is most likely due to DNA fragmentation of the G_2 cells and could be defined as a "sub-G_2 peak". A sub-G_2 peak is not evident when the analysis is performed on nuclei (Fig. 6, *top row*), where a larger sub-G_1 peak predominates. This is probably due to extraction and loss of low molecular weight DNA fragments during the preparation of nuclei from the apoptotic cells in G_2 (1, 20). Consistent with this hypothesis, nuclei preparations do not show an increased G_2/M peak.

Fixation of whole cells with paraformaldehyde allowed a better preservation of the sub-G_2 peak (Fig. 6, *bottom row*). Conforming with the previously shown increase in apoptosis at 96 h, the sub-G_2 peak is increased at this time point. The G_2 peak is decreased, also suggesting that apoptosis is depleting G_2 cells. The widened G_1 peak present in fixed cells at 96 h (Fig. 6, *bottom row*) probably represents sub-G_1 and G_1 populations similar to the one represented

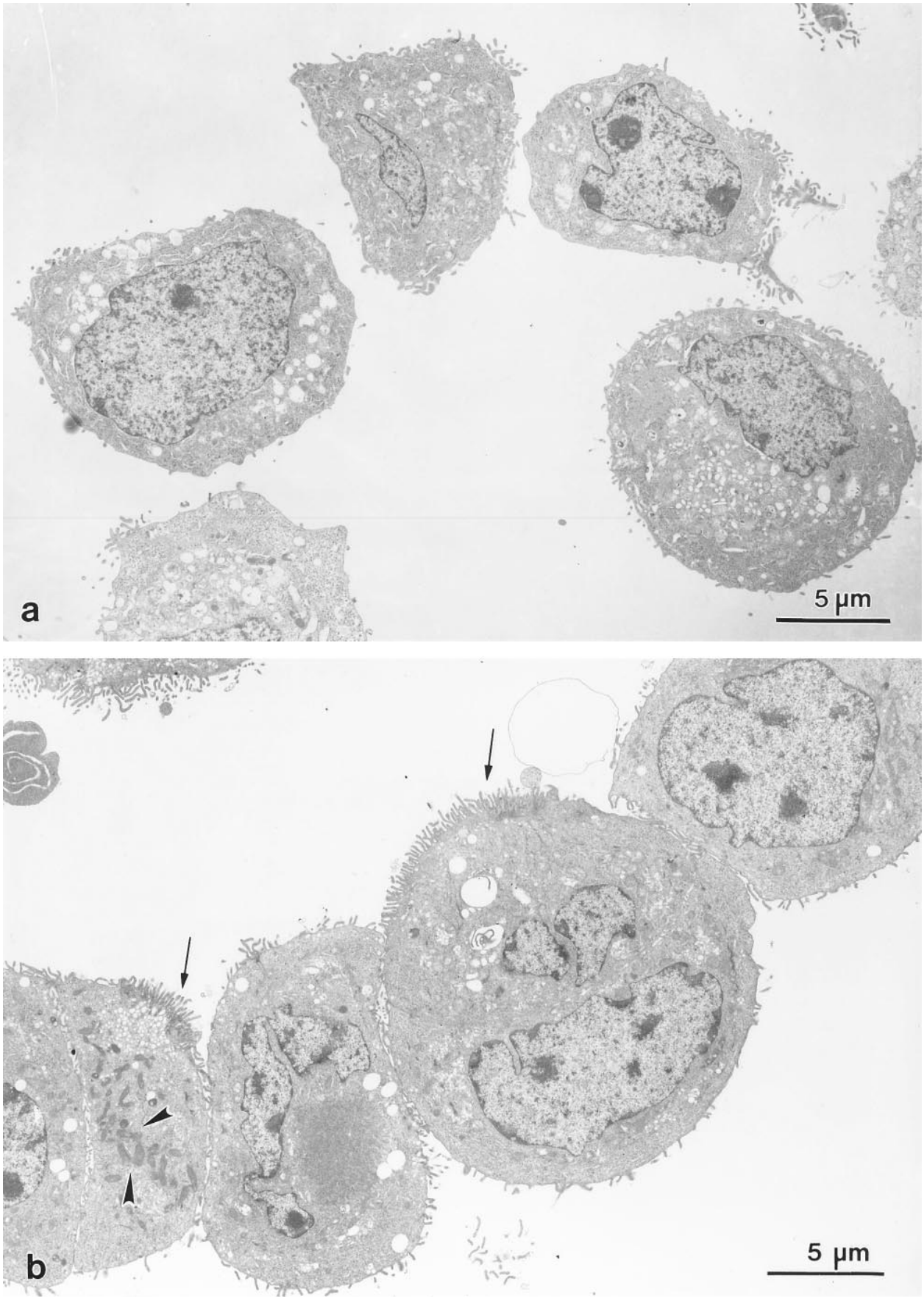

Figure 3. Transmission electron microscopy images of Colo-205 cells illustrating the differentiation process induced by in vitro exposure to herbimycin A (300 ng/ml). Untreated cells appear undifferentiated (*a*). By 24 h after herbimycin treatment (*b*), the cells tend to form a polarized monolayer with an emerging brush border (*arrows*). Some cells at this time point show increased numbers of small electron-

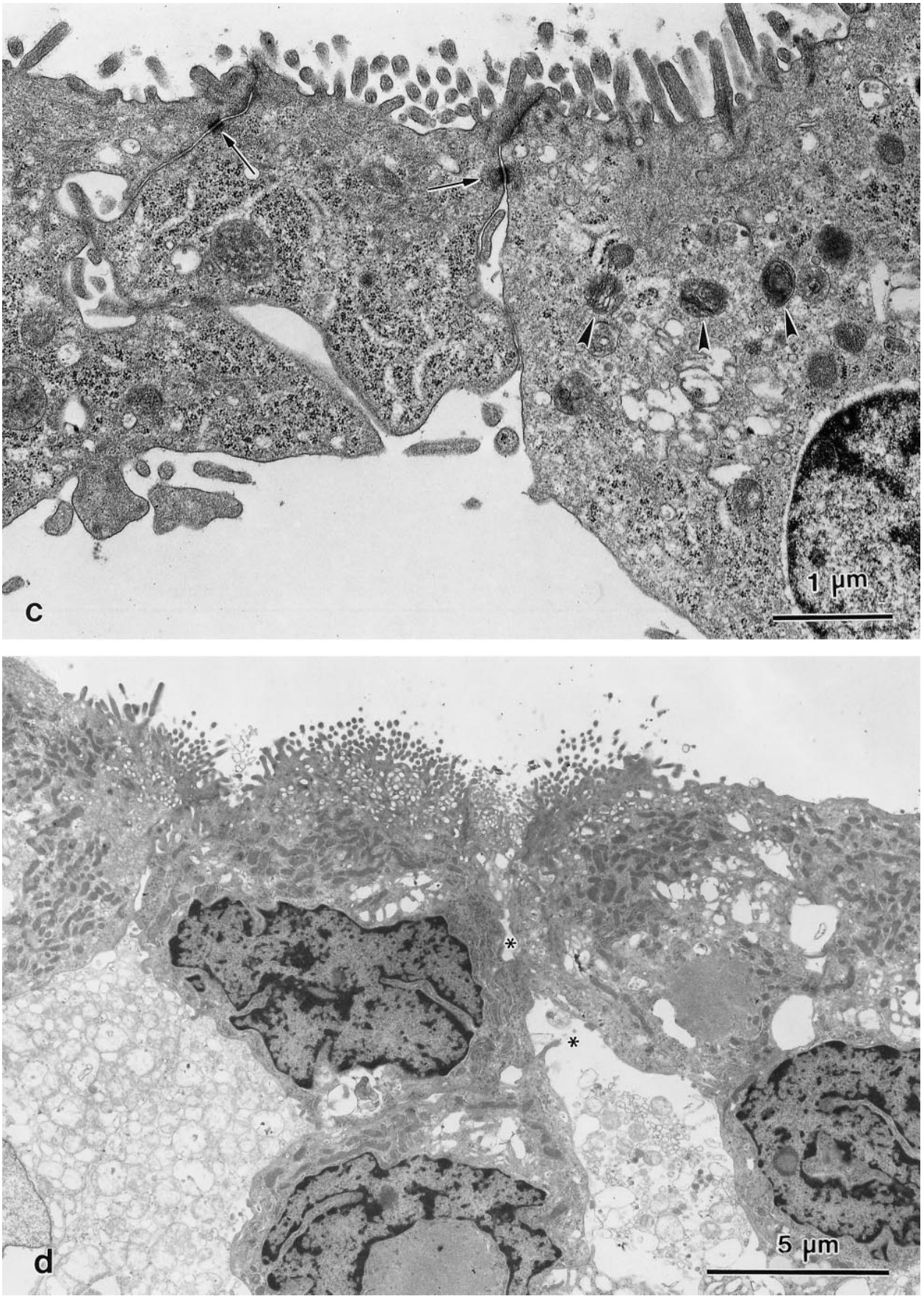

dense mitochondria (*arrowheads*). By 48 h, cells develop a more differentiated, polarized phenotype (*c*) with well formed desmosomes connecting adjacent cells (*arrows*). Some mitochondria show signs of degeneration and derangement of the membranes (*arrowheads*). At 96 h (*d*), adjacent differentiated cells show many highly condensed, small mitochondria and zones of intercellular detachment (*asterisks*).

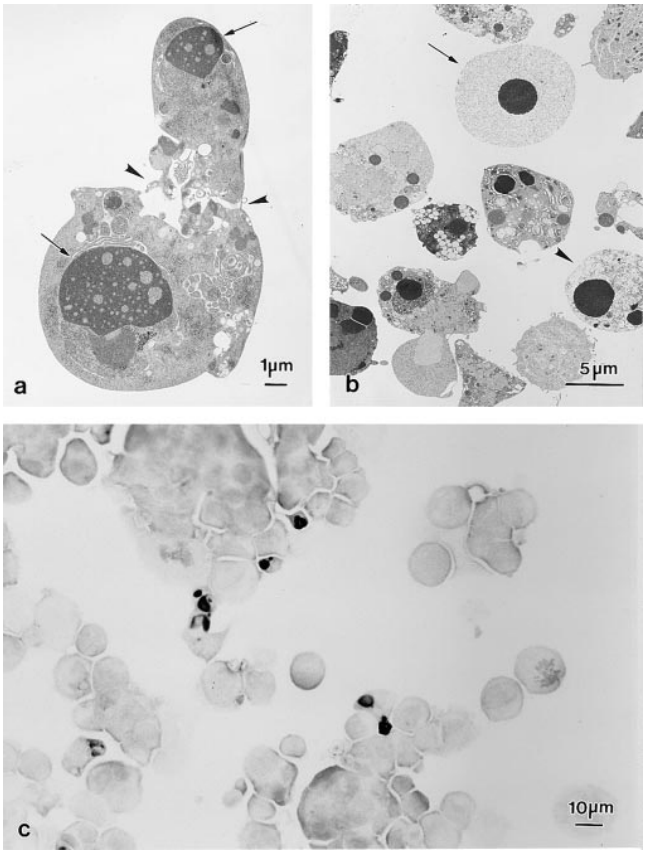

Figure 4. Electron and light microscopic images illustrating herbimycin-treated Colo-205 cells undergoing apoptosis. A whole apoptotic cell (*a*) has a mostly intact cellular membrane with cytoplasmic shrinkage and condensation. The nucleus appears pyknotic and fragmented (*arrows*). The cell also seems to be undergoing fragmentation (*arrowheads*), forming an apoptotic body. Apoptotic bodies at various stages of degeneration (*b*); some contain highly condensed chromatin (*arrowhead*), and others appear to be nuclear fragments undergoing chromatolysis (*arrow*), as in post-apoptotic necrosis. Tunel staining of Colo-205 cells at 48 h after herbimycin treatment labels apoptotic nuclei in black (*c*).

in Fig. 6, middle row. Due to software limitations, it is not possible to discriminate sub-G_1 together with sub-G_2 populations in this sample.

Simultaneous measurement of DNA content (cell cycle) and apoptotic strand breaks (DNA fluorescein-dUTP labeling) was also performed (34, 64). While absent at 0 and 24 h, TdT labeling is confined to the population of cells in G_2 and sub-G_2 at 48 h (Fig. 7). This result confirms that apoptosis begins in Colo-205 cells residing in G_2 after herbimycin treatment. By 96 h, the extensive DNA degradation may not be detectable in G_2 cells by the TdT assay of

Table I. Percentage Cytosolic DNA (Dpa Assay)

	0 h	24 h	48 h	96 h
DMSO (vehicle)	1 ± 1	4 ± 3	1 ± 1	1 ± 1
Herbimycin A	1 ± 1	5 ± 1	23 ± 5*	35 ± 4*
DMSO (vehicle) + NAC	2 ± 1	2 ± 1	2 ± 1	1 ± 1
Herbimycin A + NAC	2 ± 1	3 ± 1	2 ± 1	3 ± 1

*$P < 0.01$ vs 0 h and DMSO (all groups)

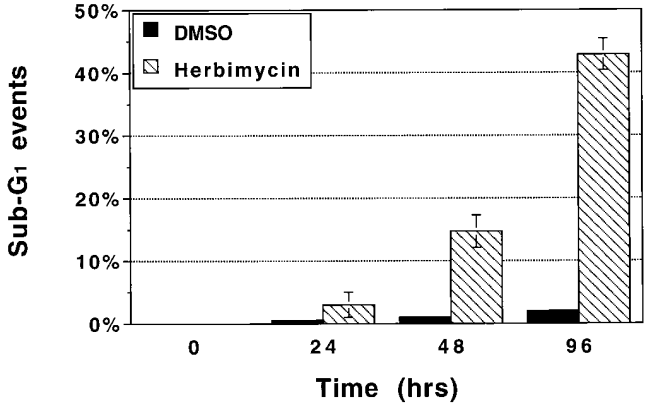

Figure 5. The frequency of sub-G_1 events (percentage of particles in the "sub-G_1 peak") obtained analyzing nuclear preparations from Colo-205 cells after 0, 24, 48, or 96 h of treatment with herbimycin A (300 ng/ml) or DMSO vehicle (1%). The increasing number of events with sub-G_1 DNA content in herbimycin-treated samples is characteristic of apoptosis.

DNA strand break labeling because very excessively fragmented, small molecular weight DNA cannot be retained in the cells and is extracted during the sample preparation (Darzynkiewicz, Z., personal communication).

Cell cycle analysis, in conclusion, shows an early decrease in S phase, with G_2 accumulation at 24–48 h and evidence of apoptosis beginning in G_2 at 48 h.

Herbimycin A Induces Increased Mitochondrial Mass but Decreased Relative Mitochondrial Transmembrane Potential

The mitochondrial abnormalities observed by electron microscopy during herbimycin-induced differentiation were further evaluated using specific fluorescent mitochondrial probes. To measure changes in mitochondrial mass, cells were stained at different time points with NAO (67), a fluorescent dye that specifically binds to the mitochondrial inner membrane independent of energetic state ($\Delta\Psi_m$). Herbimycin-treated cells showed a progressive increase in mean NAO fluorescence with time (Table II), consistent with the increased number of mitochondria per cell observed on electron microscopy. In contrast, rhodamine 123 fluorescence, an indicator of $\Delta\Psi_m$ (14, 49), did not increase after herbimycin treatment. Thus, the cellular mitochondrial transmembrane potential per unit mitochondrial mass, expressed as the ratio of rhodamine 123 to NAO fluorescence, decreased throughout the 96-h experimental period (Table II).

To control for potential differences in NAO/rhodamine 123 loading, we repeated the mitochondrial staining experiments using the J-aggregate forming lipophilic cation JC-1 (Fig. 8, *a* and *b*). This mitochondrial dye, which normally exists in solution as a monomer emitting a green fluorescence, assumes a dimeric configuration emitting red fluorescence in a reaction driven by mitochondrial transmembrane potential (94, 111). Thus, the use of JC-1 allows simultaneous analysis of mitochondrial mass (green fluorescence) and mitochondrial transmembrane potential (red fluorescence). After treatment with herbimycin we again observed a progressive dissociation between mito-

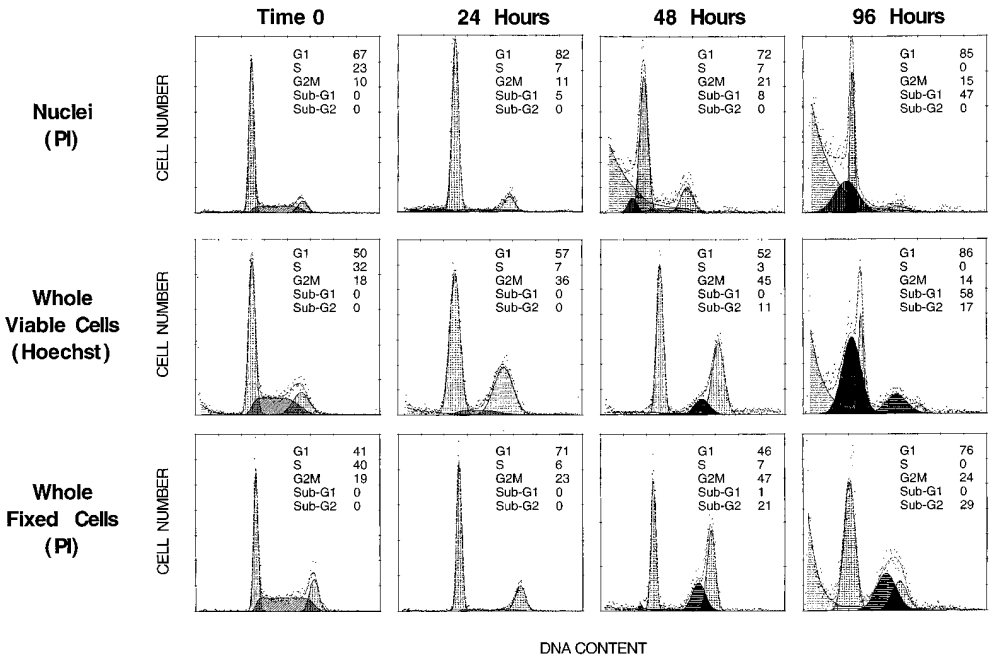

Figure 6. Cell cycle analysis of Colo-205 cells after 0, 24, 48, and 96 h of incubation with herbimycin A, as assessed by analysis of DNA content and represented in histograms plotting DNA content versus cell number. Nuclear preparations stained with propidium iodide were analyzed first (*top row*). The histograms show an early decrease in S phase and a progressively larger sub-G_1 peak, characteristic of apoptosis. Analysis of viable whole cells stained with Hoechst 33342 (*middle row*) revealed a G_2/M accumulation starting at 24 h of treatment and peaking at 48 h. At this time point, a sub-G_2 peak is detected by the computer software, suggesting beginning apoptosis in G_2/M. Fixation of whole cells with 1% paraformaldehyde, followed by propidium iodide staining, shows a better preservation of the sub-G_2 peak at 48 and 96 h (*bottom row*).

chondrial mass and $\Delta\Psi_m$, with incremental increases in JC-1 green fluorescence without a corresponding increase in JC-1 red fluorescence. Like the rhodamine 123 to NAO ratio, the JC-1 red to green fluorescence ratio decreased with time as differentiation and apoptosis progressed (Table II).

The consistent results of the mitochondrial staining experiments, while confirming the increase in mitochondrial mass observed by electron microscopy, showed a decrease in unit mitochondrial transmembrane potential. This pattern has been associated with mitochondrial uncoupling and increased mitochondrial production of ROS (127). We subsequently tested whether ROS production increased in this model.

Herbimycin A Induces Increased ROS Generation

We tested the production of ROS by staining with DHE and H_2–DCF-DA, which are oxidized in the presence of superoxide (O_2^-) and peroxides, respectively, to fluorescent products (5, 44, 99, 127). Production of O_2^- and peroxides in herbimycin-treated Colo-205 cells increased with time (Fig. 9, and Table II). At 24 h, before detection of apoptosis, an increase in ROS production was already apparent, corresponding to the first decrease in the ratio of JC-1 red and green fluorescence. This correlation was maintained at later times, as the population continued to show an increase in ROS production and a proportional decrease in JC-1 red to green ratio (Fig. 9, and Table II).

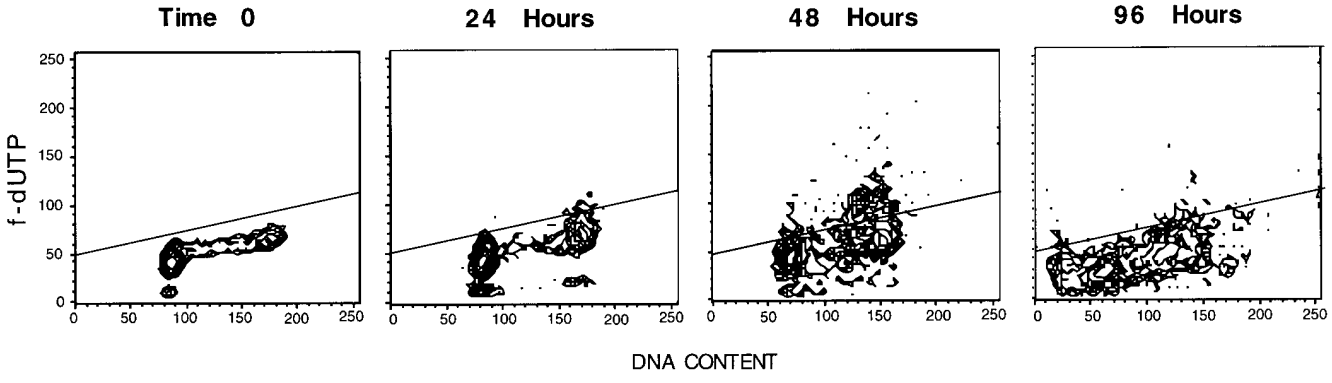

Figure 7. TdT flow cytometry of Colo-205 cells after 0, 24, 48, and 96 h of incubation with herbimycin A. The graphs plot DNA content on the x-axis and TdT-labeled apoptotic DNA strand breaks on the y-axis. No increase in TdT labeling above baseline is apparent at 24 h after addition of herbimycin. By 48 h, a population of cells with increased TdT-labeling is present, corresponding to the cells with DNA content in the sub-G_2 and G_2/M phase of the cell cycle. By 96 h, extensive DNA loss due to massive cell death is represented as a shift to the left on the DNA histogram, preventing significant TdT labeling at this time point.

Table II. Mean Fluorescence Values of Mitochondrial Mass, $\Delta\Psi_m$, and ROS Production in Herbimycin-treated Cells (Relative to DMSO Control Cells)

	0 h	24 h	48 h	96 h
NAO	1	1.5 ± 0.3*	1.6 ± 0.3*	1.8 ± 0.5*
Rhodamine	1	1.1 ± 0.1	1.1 ± 0.3	0.7 ± 0.2
Rhodamine/NAO	1	0.7 ± 0.3	0.6 ± 0.2*	0.4 ± 0.2*
JC-1 green	1	1.5 ± 0.1*	1.7 ± 0.1*	3.0 ± 0.3*
JC-1 red	1	1.0 ± 0.1	1.0 ± 0.3	1.0 ± 0.2
Red/green	1	0.7 ± 0.1*	0.6 ± 0.2*	0.3 ± 0.1*
O_2^- (DHE)	1	1.3 ± 0.1	1.6 ± 0.3*	1.8 ± 0.4*
H_2O_2 (DCFH)	1	2.5 ± 0.6	3.0 ± 1.1*	4.0 ± 1.7*

*$P \leq 0.05$ vs 0 h.

Sequence of Ultrastructural Changes in Mitochondria during Herbimycin Exposure

Sequential changes in mitochondrial ultrastructure were identified in differentiating Colo-205 cells by electron microscopy. On the electron micrographs, the extent of nuclear chromatin condensation can be correlated with changes in mitochondrial number and structure within the same cell. Before addition of herbimycin, the mitochondria appear oval shaped, with a finely granular matrix containing a few dense granules (Fig. 10 *a*). The cristae are sparse, and the mitochondria are occasionally adjacent to endoplasmic reticulum cisternae.

24 h after addition of herbimycin, the increase in mitochondrial number is associated with more elongated forms. The matrix is condensed, and the cristae are well formed, often traversing the mitochondrion. Wide cisternae of rough endoplasmic reticulum are wrapped around mitochondria, and a general increase in the number of polysomes in the cytoplasm is observed (Fig. 10 *b*). This feature suggests an increase in protein synthesis and mitochondrial import during the early stages of herbimycin-induced apoptosis. Lysosome-like vacuoles containing myelin figures are sometimes seen juxtaposed to mitochondria/rough endoplasmic reticulum complexes and may represent ongoing autophagocytosis of damaged organelles (33). Nuclear chromatin in the cells appears normal at this stage.

As differentiation proceeds through 48 h, the mitochondria become more numerous, small and condensed, while the associations with rough endoplasmic reticulum cisternae progressively decrease (not shown). Deranged cristae suggest the development of mitochondrial degeneration (Fig. 3 *c*). Overall these changes are suggestive of extensive mitochondrial proliferation, coupled with matrix condensation and volume loss.

Mitochondrial ultrastructure in differentiated cells at 96 h is characterized by hypercondensation of the matrix and further reduction in size, with high numbers of mitochondria packed in the cytoplasm (Fig. 11 *a*). The outer mito-

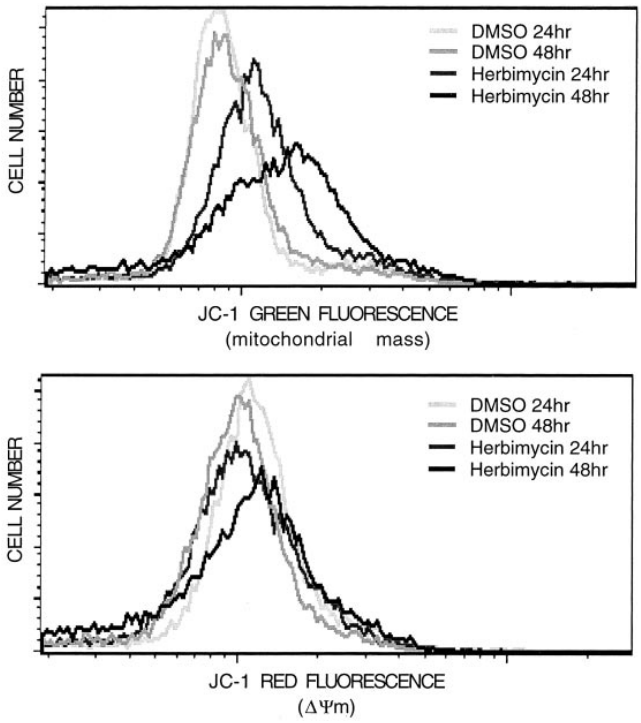

Figure 8. JC-1 fluorescence in Colo-205 cells after 24 and 48 h of incubation with herbimycin A or DMSO vehicle. JC-1 green fluorescence (*mitochondrial mass*) increases with time while JC-1 red fluorescence ($\Delta\Psi_m$) remains relatively unchanged. These findings suggest that herbimycin induces proliferation of mitochondria with decreased net transmembrane potential per unit mitochondrial mass.

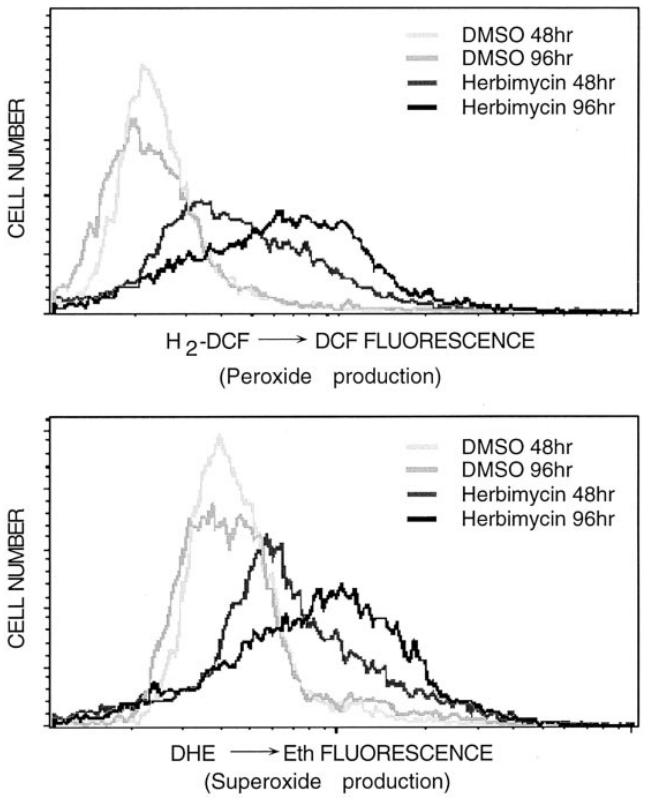

Figure 9. H_2–DCF-DA → DCF and DHE → Eth fluorescence in Colo-205 cells after 48 and 96 h of incubation with herbimycin A. Herbimycin-treated cells demonstrate progressively increasing ROS production as compared with the DMSO controls. Peak ROS production is concomitant with maximal induction of apoptosis at 96 h.

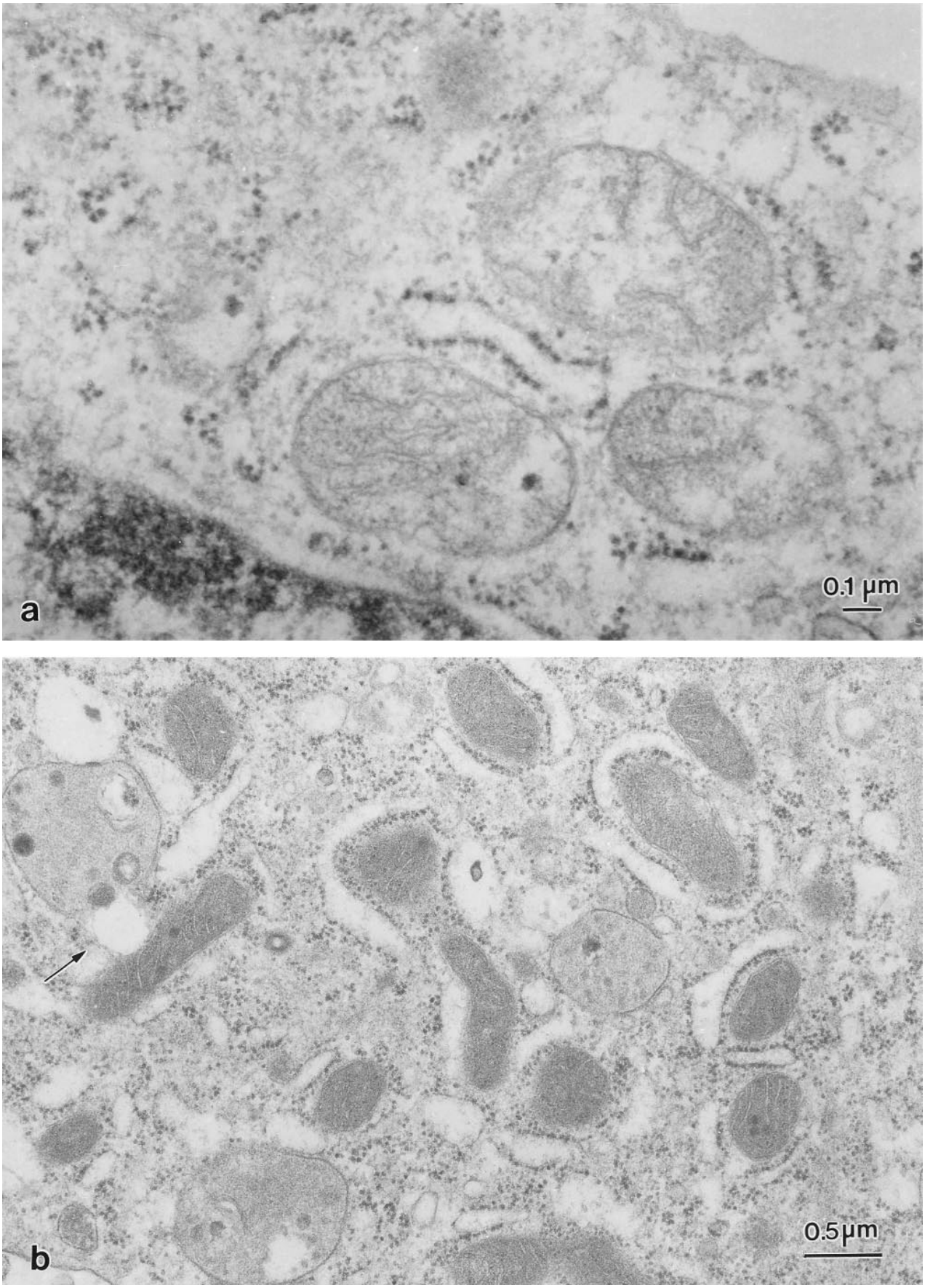

Figure 10. High magnification electron microscopy images of Colo-205 cells before (*a*) and after (*b*) 24 h of herbimycin treatment. Change in mitochondrial morphology is characterized by condensation of the matrix and markedly increased association with wide cisternae of rough endoplasmic reticulum. Lysosome-like vacuoles adjacent to mitochondria (*arrow*) suggest ongoing autophagocytosis.

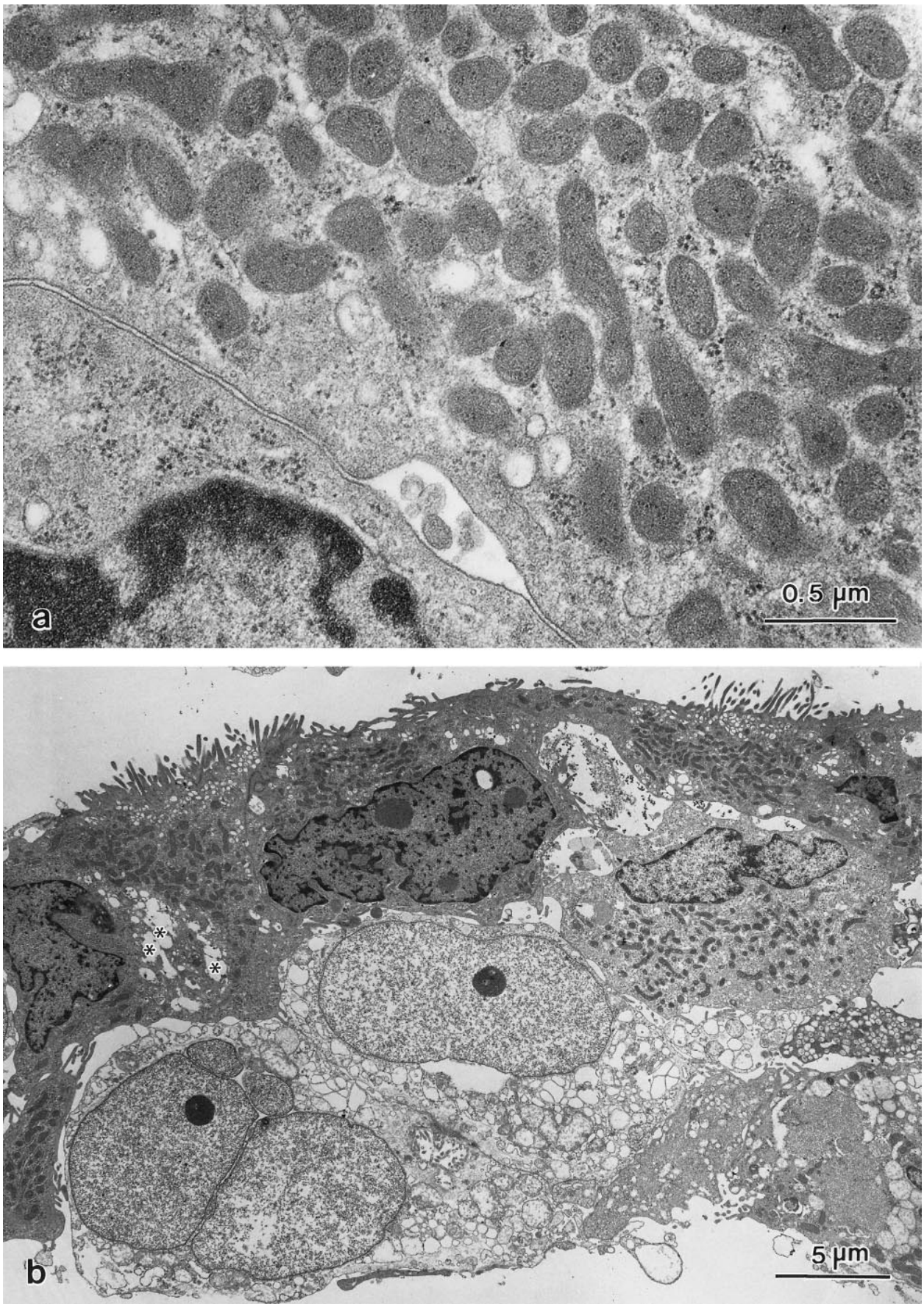

Figure 11. High and low magnification electron microscopy images of Colo-205 cells after 96 h of herbimycin treatment. Mitochondria appear increased in numbers, hypercondensed, and small. The association between mitochondria and the cisternae of rough endoplasmic reticulum is decreased (*a*). At lower magnification this mitochondrial morphology is observed in apical differentiated cells (*b*) de-

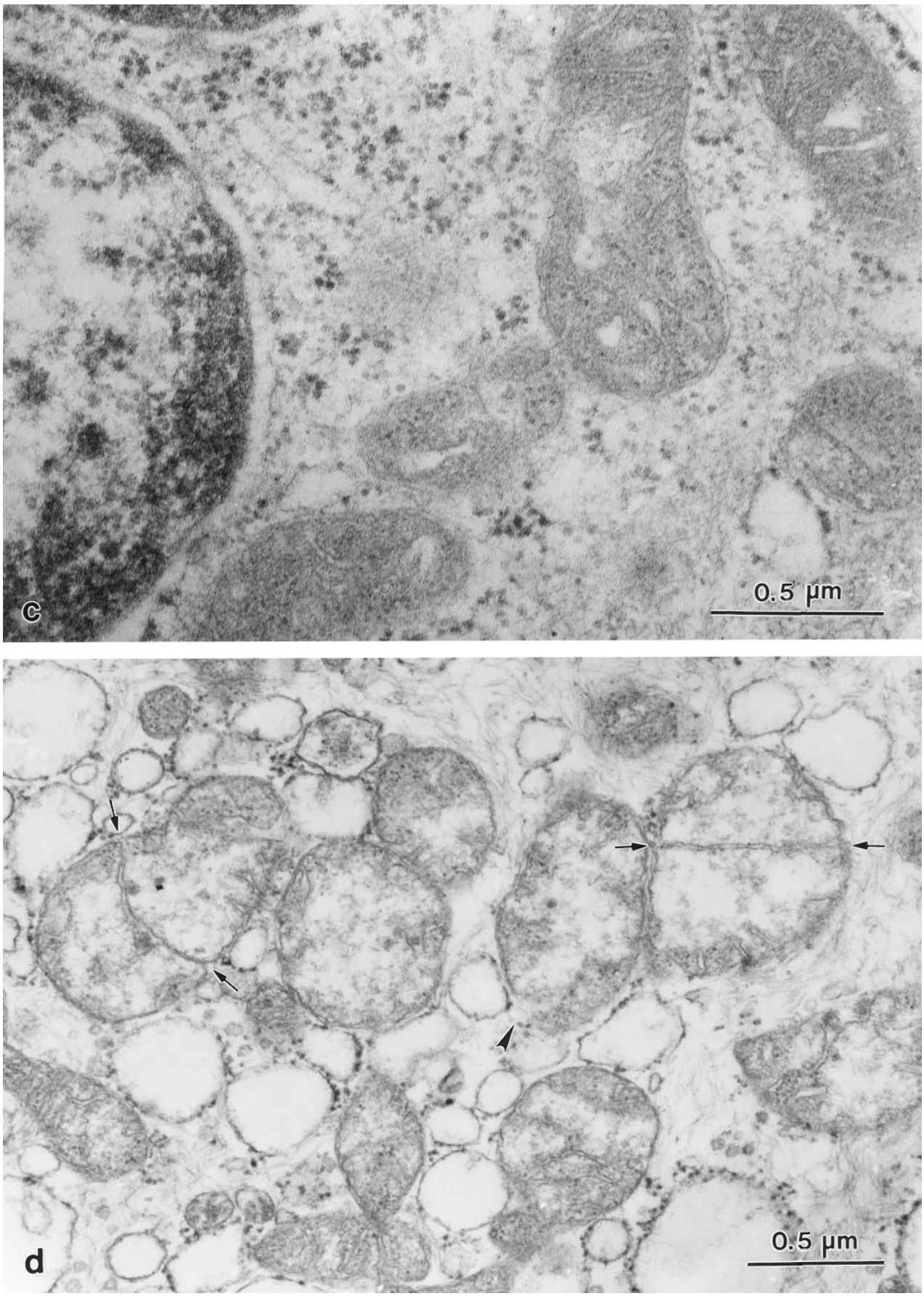

taching from the neighboring cells (*asterisks*). Subsequent mitochondrial degeneration is characterized by intracristal ballooning (*c*) followed by mitochondrial swelling (*d*) with interruption of the mitochondrial membrane (*arrowhead*) and profiles suggestive of mitochondrial division (*arrows*).

Table III. Mean Fluorescence Values of Mitochondrial Mass and $\Delta\Psi m$ in Herbimycin + NAC-treated Cells (Relative to DMSO + NAC Control Cells)

	0 h	24 h	48 h	96 h
JC-1 green	1.0	1.0 ± 0.1	1.0 ± 0.1	1.3 ± 0.7
JC-1 red	1.0	1.2 ± 0.1	0.9 ± 0.3	1.1 ± 0.5
Red/green	1.0	1.2 ± 0.2	0.9 ± 0.3	0.8 ± 0.1

P = NS.

chondrial membrane appears indistinct, and internal structures are obscured by the highly electron-dense matrix. The close association between mitochondria and rough endoplasmic reticulum is no longer seen. The nuclear chromatin at this stage is condensed and marginated.

Finally, a spectrum of degenerative changes is noted in the mitochondria of cells in advanced apoptosis 96 h after treatment with herbimycin. This pattern is characterized by mitochondrial swelling and loss of matrix density. The nuclear chromatin and the cytoplasm are also less condensed, and many cells have a morphological appearance characteristic of post-apoptotic necrosis (Fig. 11 *b*). As the nuclear chromatin appear less condensed, the mitochondria show enlargement of the cristae (intracristal swelling or ballooning). The matrix appears still condensed, but to a lesser degree than before, while the total mitochondrial volume does not appear increased (Fig. 11 *c*). Chromatolysis is associated with a more advanced mitochondrial pathology (Fig. 11 *b*). Widening of the intracristal space becomes more evident, and the mitochondria show a high degree of swelling and appear electron lucent and more rounded (Fig. 11 *d*). The matrix contains flocculent densities, and the outer membrane is often discontinuous. The internal mitochondrial structure becomes visible again and shows some cristae dividing the organelle into two symmetric halves (partition), a feature suggestive of mitochondrial division (33).

NAC Prevents Herbimycin-induced Mitochondrial Changes and Protects the Cells from Apoptosis

We subsequently tested the effect of NAC on Colo-205 cells exposed to herbimycin. NAC has been previously shown to protect cells against damage associated with oxidative stress (3, 73, 74, 113). Colo-205 cells treated with a combination of 500 μM NAC and herbimycin A did not undergo apoptosis (Table I). Herbimycin-induced epithelial differentiation was not affected by NAC, as judged by light and electron microscopic inspection. However, mitochondrial proliferation in response to herbimycin was abolished by co-treatment with NAC. JC-1 green fluorescence and the ratio of red to green fluorescence intensities remained at baseline values under these conditions (Table III). The absence of mitochondrial changes was confirmed by EM, demonstrating a lack of change in mitochondrial number and morphology, despite the development of a characteristic differentiated cellular phenotype (not shown).

Mitochondria-enriched Fractions Are Required for Apoptotic Activity of Colo-205 Lysates

As a further indicator of the relationship of mitochondrial changes to the apoptotic program, we tested whether apoptotic "activity" in cell-free assays showed an early dependence on mitochondria from Colo-205 cells. Using rat liver nuclei to score apoptotic responses, cytosolic extracts were prepared from Colo-205 cells exposed to herbimycin for 0, 24, and 48 h. Extracts were incubated with the nuclei for 1 h at 37°C. Extracts of Colo-205 cells at time 0 did not show apoptotic activity (Fig. 12 *a*). In contrast, cytosolic extracts of cells treated with the drug for 24 h induced classical changes of apoptosis in the target nuclei after 1-h incubation at 37°C (Fig. 12 *b*). We removed a heavy membrane fraction containing mitochondria from cell lysates, by centrifugation at 10,000 *g* for 30 min. The S10 supernatant at 24 h had no demonstrable apoptotic activity in the cell-free assay even after 2 h of incubation with nuclei (Fig. 12 *c*). 48-h extracts showed similar apoptotic activity to the 24-h samples, but the corresponding S10 supernatant was still able to induce partial apoptotic responses in the target nuclei (not shown). These results indicate that at 24 h, before irreversible activation of cytoplasmic components, the apoptotic program induced by herbimycin requires the early action of mitochondria.

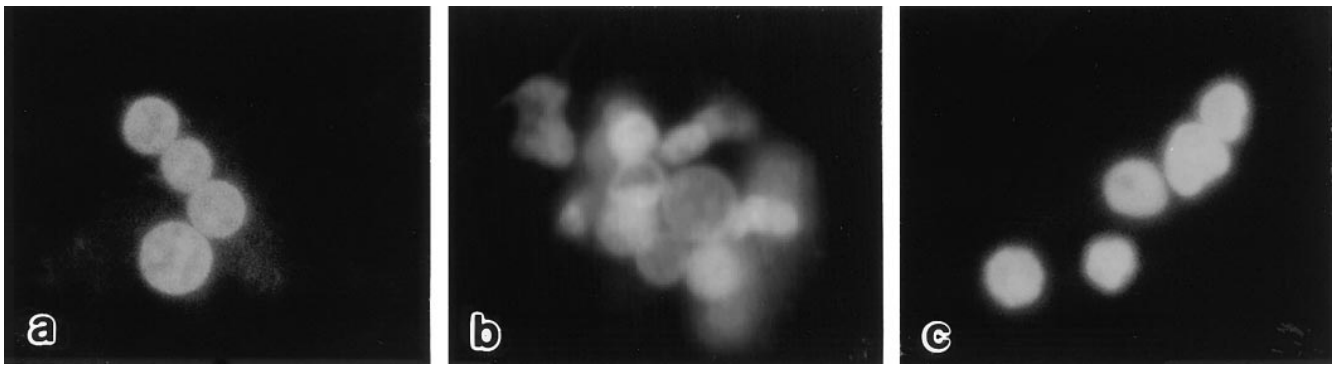

Figure 12. Cell free assay for apoptosis incubating rat liver nuclei with cytosolic extracts from Colo-205 cells. Colo-205 extracts (protein concentration 5 μg/ml) were incubated with rat liver nuclei for 1 h (37°C) and then visualized by fluorescence microscopy after DNA staining (Hoechst 33258). (*A*) Nuclei exposed to cytosolic extract of untreated Colo-205 cells appear normal. (*B*) Nuclei exposed to cytosolic extract of Colo-205 cells treated with herbimycin for 24 h show chromatin margination and condensation. (*C*) Nuclei exposed to S10 fraction from Colo-205 cells treated with herbimycin for 24 h show normal morphology.

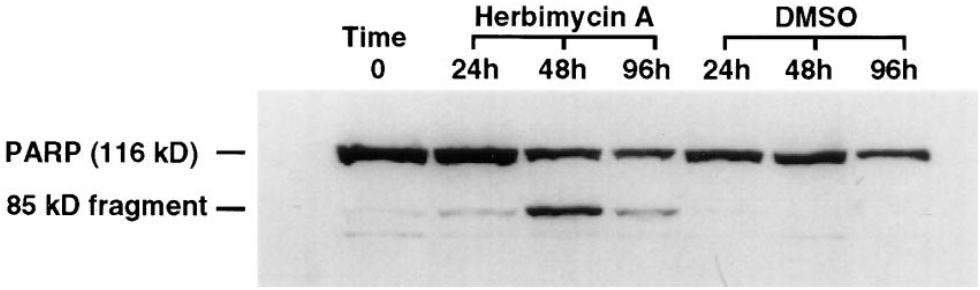

Figure 13. Western blot detection of PARP in Colo-205 cells at time 0 and after treatment with herbimycin A or vehicle for 24, 48, and 96 h. Cleavage of PARP (116 kD) yields the 85-kD fragment detectable at 48 and 96 h of herbimycin exposure. PARP cleavage is not detected in untreated cells (time 0) or the DMSO-treated control cells. The faint 85-kD band seen in the herbimycin cells 24 h after treatment is a result of increased protein loading in this lane and was not observed in two other runs of the same experiment.

Herbimycin-induced Mitochondrial Changes Precede PARP Cleavage

To assess the activation of ICE family members in Colo-205 cells, we examined cleavage of PARP, a proteolytic target of the CPP32/Yama protease (81, 115). Cleavage of PARP to an 85-kD fragment has been described as an early event in drug-induced apoptosis in mammalian cells (51). The 85-kD proteolytic fragment of PARP was first detected in immunoblots of Colo-205 lysates after 48 h of exposure to herbimycin A (Fig. 13). Changes in mitochondrial morphology, as well as an increase in mitochondrial numbers and a decrease in the JC-1 red/green ratio have already occurred by 24 h (Figs. 8 and 10 *b*, and Table II), preceding PARP cleavage.

Discussion

The nonspecific tyrosine kinase inhibitor herbimycin A can induce differentiation in several experimental models (45, 120). Experimentally transformed cell lines treated with herbimycin can also transiently revert to an untransformed phenotype (76, 118, 120, 121). We have been studying herbimycin-induced epithelial differentiation in the human colon cancer cell line Colo-205, associated with inhibition of *src* and *lck* tyrosine kinase activities (Paty, P., and N. Rosen, unpublished observations).

In the present study we report that, in addition to differentiation, herbimycin induces apoptotic cell death in Colo-205 cells. Moreover, the two events occur sequentially. Differentiation starts 24 h after herbimycin exposure and appears fully developed at 48 h, while apoptosis becomes detectable at 48 h and peaks at 96 h. This relationship between differentiation and apoptosis in Colo-205 cells appears to mirror the changes occurring in normal colonic mucosa during the physiologic program of terminal differentiation of enterocytes (15, 77). The undifferentiated stem cells localized at the base of colonic crypts give rise to daughter cells that differentiate and migrate up the crypt to reach the mucosal surface, where they die by apoptosis and are sloughed from the colonic surface (32, 90). The physiologic life span of the differentiating cells lasts about 3–5 d (15). Terminal differentiation in the immortalized undifferentiated cell line Colo-205 after in vitro exposure to herbimycin is also followed by apoptosis after a similar time lag, suggesting that the enterocyte pathway of terminal differentiation and apoptosis are tightly linked. In our model, we also observe that a small number of cells undergo apoptosis as early as 24 h. This is consistent with findings in normal intestine where scattered apoptotic cells are detected at multiple levels of the crypt–villus axis, including occasional cells adjacent to the crypt bases (90, 107).

Herbimycin A also induces an accumulation of Colo-205 cells in the G_2/M phase of the cell cycle. Apoptosis seems to occur preferentially in G_2/M, as demonstrated by the presence of a sub-G_2 apoptotic peak and of positive TdT labeling of G_2/M cells (20, 34). Another tyrosine kinase inhibitor, genistein, has been shown to induce G_2 arrest in vitro (72). We have also observed that genistein induces in Colo-205 cells G_2 arrest, differentiation, and apoptosis, similar to herbimycin (Mancini, M., and B. Anderson, unpublished observations). Roche et al. showed that signal transduction pathways involving tyrosine kinases function in mitosis, in particular, *src* family kinases are required for the G_2–M transition (98). As a consequence, one of the direct effects of herbimycin could be to arrest the cells in the G_2 phase of the cell cycle.

Terminal differentiation normally occurs when the cells exit the cell cycle and arrest in G_1 (27). However, a G_1 arrest may not be necessary for commitment to terminal differentiation. A number of drugs known to cause a cell cycle delay in G_2 are able to induce terminal differentiation in murine Friend erythroleukemia (FEL) and K562 leukemia cells (24, 130).

Besides typical apoptotic cells and apoptotic bodies, we also observed in our EM preparations, particularly at 96 h, some cells with a phenotype characteristic of cellular necrosis, i.e., chromatolysis, cytoplasmic vacuolization, and disruption of the cellular membrane. We interpret this cellular morphology as a secondary event to apoptosis, or "post-apoptotic necrosis," as recently proposed by Majno and Joris (68). The appearance of a necrotic morphology after apoptosis has been described in embryonic tissues and in dermatopathology (103, 125). Even in the classical model of apoptosis induction described by Kerr, the ligation of the main portal venous trunk to the left and median lobes of the rat liver with consequent liver atrophy and formation of Councilman bodies, these are found to sometimes

undergo severe degenerative changes resembling necrosis (52, 53). A possible apoptosis–necrosis sequence has also been recently reported in dystrophin-deficient muscle cells, previously believed to die primarily by necrosis (116). It is not known whether post-apoptotic necrosis occurs during the late stages of terminal differentiation of normal enterocytes. Phagocytosed apoptotic bodies in various stages of lysosomal digestion have been observed in the stratified colonic mucosa of rat embryos (38), but in a study by Potten and Allen on adult mouse small intestinal mucosa, phagocytosis and cellular fragmentation were seen only in cells dying at lower positions along the crypt–villus axis, with a less differentiated phenotype (90). Terminally differentiated cells were shown to be shed at the villus tip after loss of contact with the neighboring cells, without undergoing phagocytosis. Early apoptotic changes, such as nuclear pyknosis and chromatin margination were observed in terminally differentiated enterocytes, but they were mostly extruded as whole cells (90). It is possible that later, once in the bowel lumen, they undergo further degeneration in the form of post-apoptotic necrosis.

Our results show that herbimycin-induced differentiation in Colo-205 cells is associated with an increase in mitochondrial number but without a concomitant increase in net mitochondrial transmembrane potential. These results suggest an accumulation of mitochondria with low transmembrane potential. There is scant information available on the role of mitochondria during terminal differentiation programs. Studies by Heerdt and colleagues have reported increased mitochondrial gene expression in colon carcinoma cells after induction of differentiation along the absorptive lineage (39) and that increased mitochondrial gene expression is a consistent and early event during apoptosis of colonic carcinoma cells in vitro (40). The importance of mitochondrial abnormalities during apoptosis has been gaining support recently (41), despite the classical descriptions of apoptosis with morphological preservation of mitochondria (53). The availability of fluorescent dyes which specifically reflect mitochondrial mass and function has enabled more detailed studies of mitochondrial modifications during apoptosis (87). Vayssiere et al. have shown in rat embryo fibroblasts transfected with a temperature-sensitive mutant of SV40 T antigen that reduction of $\Delta\Psi_m$ is an early event during apoptosis triggered by inactivation of SV40 T antigen (123). Petit et al. have reported similar results in dexamethasone-induced apoptosis of murine thymocytes (89). Apoptosis in peripheral lymphocytes from mice treated with dexamethasone is correlated with an early reduction in $\Delta\Psi_m$, while classical nuclear features of apoptosis are not detectable in vivo (127).

The increase in mitochondrial number during herbimycin-induced differentiation in Colo-205 cells is associated with condensation of the mitochondrial matrix and a reduction in total mitochondrial volume. This condensed appearance is notable at early time points in Colo-205 cells, before apoptotic changes in the nucleus. The degree of mitochondrial condensation subsequently increases in concert with the appearance of chromatin and cytoplasmic condensation. At later time points, signs of mitochondrial degeneration are apparent, characterized initially by dilatation of the intracristal space and then by progressive swelling of the mitochondria, with interruption of the outer membrane and loss of matrix density. This sequence of mitochondrial modifications in Colo-205 cells after herbimycin treatment, represented in Figs. 10 and 11, shows a transition from an orthodox, to condensed, to transitional, and finally to swollen conformation (33). Transitional and swollen morphologies are associated with progressive chromatolysis and necrotic degeneration of the cells.

Morphological studies by Hackenbrock and colleagues have shown that a reversible transition of mitochondrial morphology from an orthodox to a condensed conformation is associated with high and low energy states of mitochondria, respectively (35–37). The condensed morphology is characterized by a reduction in the inner mitochondrial compartment due to increased folding of the inner membrane, with a consequent increase of the outer compartment, intracristal space and without significant reduction of the total mitochondrial volume. Further studies on mitochondrial morphology in response to inhibition of ATP synthesis or cellular injury published by Laiho and colleagues demonstrated a sequence of mitochondrial modifications from the orthodox, to condensed, and eventually to swollen mitochondrial conformations (60, 61). A transitional morphology characterized by increased intracristal space can also be observed between the condensed and the swollen configuration. In these studies the condensed conformation, due to loss of water and ions from the mitochondrial inner compartment, was associated with decreased ATP synthesis, with or without decreased respiration, while the swollen conformation represents a more advanced stage of damage to the inner mitochondrial membrane and is usually associated with cellular necrosis. The condensed conformation was reversible before the "point of no return" is reached. Nevertheless the condensed conformation is unstable, and, in situations of continued injury, the mitochondrial membrane becomes permeable and the organelle swells progressively, with rupture of the outer membrane and destruction of the different components (60, 61). The appearance of a mitochondrial condensed morphology, followed by progressive mitochondrial swelling, has also been recently reported by Papadimitriou et al. to occur during complement-mediated cell death in Ehrlich ascites tumor cells (85).

The sequence of mitochondrial alterations observed in herbimycin-treated Colo-205 cells differs in some respects from that observed by Laiho and Trump (60). At a time when the degree of mitochondria condensation in Colo-205 cells is advanced, the outer and inner mitochondrial membranes appear closely associated, the intracristal space is not enlarged, and the total mitochondrial volume is reduced. This morphology could be described as "mitochondrial pyknosis," characterized by hyperdensity of the matrix and reduction in mitochondrial size (33). It is possible that in our model the pyknotic configuration represents a more extensive and pathological degree of mitochondrial condensation, with contraction of the outer mitochondrial membrane. Mitochondrial pyknosis has been sporadically reported in the literature (30, 69, 100, 101, 114). The term was first employed by Wachstein and Besen in a study of renal tubular coagulative necrosis due to dl-serine intoxication in rats (124). It is interesting to observe that in this paper, published before the first paper on apoptosis by Kerr et al. (53), early focal lesions were identified in which

isolated cells showed cytoplasmic condensation, nuclear shrinkage with serrated irregular outlines, and preservation of cellular membranes, aspects now recognized as "apoptotic."

The appearance of mitochondrial pyknosis is associated with activity in Colo-205 cell lysates after herbimycin exposure and could therefore represent the morphological correlative of the "point of no return" during the apoptotic pathway. An example of apoptotic mitochondrial morphology resembling mitochondrial pyknosis was reported in cardiac sinus node myocytes in patients with long QT syndrome and defined as "pleomorphic micromitochondriosis" (48). In this study, mitochondrial pyknosis was also associated with mitochondrial proliferation. Cupler et al. reported mitochondrial proliferation and ultrastructural abnormalities similar to mitochondrial pyknosis to be the earliest detectable lesion in zivudine (AZT)-associated myopathy in HIV-infected patients (19). These mitochondrial abnormalities could be one of the mechanisms leading to muscular atrophy, characteristic of more advanced stages of AZT-associated myopathy, through apoptosis. A recent study by Reipert et al. also described mitochondrial proliferation as an early response to treatment of the hematopoietic stem cell line FDCP mix with the topoisomerase II inhibitor etoposide, which induced G_2 arrest and apoptosis (95). The increase in mitochondrial mass in this model was not associated with mitochondrial pyknosis. The fact that in this study the mitochondria became targets for autolytic digestion suggests however that they may be defective.

Colo-205 cells showed increased ROS production after herbimycin treatment. This response was preceded by mitochondrial proliferation and loss of net mitochondrial transmembrane potential and peaked at 96 h along with maximal induction of apoptosis.

This sequence suggests a possible role of ROS as mediators of the apoptotic response to herbimycin. Mitochondria could be a main target of nonspecific damage through oxidative stress at the level of the outer and inner membranes (12, 44). This mechanism has been described for the elimination of mitochondria during the physiologic maturation of reticulocytes into erythrocytes, which do not contain mitochondria. Reticulocytes eliminate these organelles through the glycoprotein lipooxygenase, which causes a disruption of both mitochondrial membranes by oxidation of phospholipids in the outer and inner membranes (92, 105). As a consequence of oxidative membrane damage, membrane potential and permeability-barrier function are impaired, leading to further mitochondrial damage. Recently, oxidative damage to the mitochondrial membrane due to increased generation of ROS has been shown to play a role in apoptosis of thymocytes and bone marrow cells in a murine model of Down's syndrome (86). Similar ROS-mediated mitochondrial membrane damage has been detected as a possible cause of apoptosis in Down's syndrome human fetal cortical neurons (11). Mitochondria have also been implicated as a source of ROS during apoptosis. Reduced mitochondrial membrane potential has recently been shown to lead to increased generation of ROS and apoptosis in dexamethasone-primed murine splenocytes in vivo (127). Mitochondria are the main source of cellular ROS (9, 117).

Mitochondrial dysfunction could also be more specifically programmed or targeted. There is precedent for the activation or upregulation of specific agents of mitochondrial dysfunction in the mitochondrial uncoupling protein present in brown fat adipocytes (80). This protein is a membranous proton carrier that induces uncoupling of mitochondrial respiration from ATP production by introducing a proton-conducting pathway through the mitochondrial inner membrane, with consequent decrease in mitochondrial transmembrane potential, reduced ATP phosphorylation, and dissipation of energy as heat (96). The activity of a mitochondrial uncoupler could be particularly effective when its activation is linked to mitochondrial proliferation, with consequent accumulation of dysfunctional mitochondria and massive production of ROS. In agreement with this hypothesis, NAC, a compound previously shown to protect cells against damage associated with oxidative stress (3, 73, 74, 113) protected Colo-205 cells from herbimycin-induced apoptosis, without affecting herbimycin-induced differentiation. However, mitochondrial proliferation and pyknosis in response to herbimycin were also abolished by cotreatment with NAC, underlining the importance of unbalanced mitochondrial proliferation and dysfunction in the apoptotic response in Colo-205 cells. This unexpected result appears to provide evidence for a redox-sensitive factor that governs the mitochondrial proliferation response.

Another targeted mechanism for diminished mitochondrial function might involve the opening of the mitochondrial permeability transition pores (7, 46, 129). Mitochondrial permeability transition has been recently proposed as a critical early event in the apoptotic process (57, 70, 128).

It is also possible that mitochondria in herbimycin-treated Colo-205 cells are defective at a biosynthetic level. An example of this mechanism is the mitochondrial abnormalities, mentioned above, in the zivudine (AZT)-induced myopathy in HIV-positive patients (19). Zivudine induces inhibition of the mitochondrial DNA polymerase γ, with consequent mitochondrial DNA depletion, reduced synthesis of mitochondrial subunits, and mitochondrial dysfunction (2, 75, 110). Mitochondrial proliferation may function as a compensatory response (4) that, because of the biosynthetic defect, is not sufficient to restore an adequate mitochondrial function and leads to an accumulation of dysfunctional mitochondria (19). Another experimental model showing the deleterious effect of interference with mitochondrial biosynthesis was reported by Garden et al. (31). Neurons of the neonatal chick cochlear nucleus undergo cell death after afferent deprivation via removal of the cochlea, preceded by increased oxidative metabolism and mitochondrial mass (47, 102). Inhibition of mitochondrial protein synthesis, by in vivo administration of chloramphenicol, increases cell death after deafferentation (31). Vayssiere et al. have also shown that reduction in $\Delta\Psi_m$ during apoptosis can be associated with reduction in mitochondrial translation (123).

Cell-free assays for apoptosis enable testing of the contribution of individual subcellular components or fractions, exceeding the experimental possibilities using intact cells (62). In addition, the temporal dependence of apoptosis on specific components can be examined (25, 54, 65, 71, 79). Our results show that subcellular fractions enriched in mitochondria are required for the apoptotic ac-

tivity of lysates from Colo-205 cells treated for 24 h with herbimycin. At later time points, latent apoptotic factors in the cytosol are activated, and a strong mitochondrial dependence is no longer observed. Therefore, the apoptotic program induced by herbimycin requires the early action of mitochondria. Previous studies have shown a requirement for mitochondria in cell-free assays of apoptosis using extracts from *Xenopus* oocytes (79) or hepatocytes or lymphoid cells triggered to undergo apoptosis (128).

We also found evidence for the early timing of mitochondrial changes in herbimycin-induced apoptosis by examining their relationship to PARP cleavage. Cleavage of PARP, a proteolytic target of the CPP32/Yama protease (81, 115), has been described as an early event in drug-induced and other models of apoptosis in mammalian cells (25, 29, 51, 63, 106). Our results indicate that morphological and functional mitochondrial changes, as well as increase in ROS production, occur before detectable PARP cleavage. A similar result was reported in a recent study of cell death induced by respiratory chain inhibitors, etoposide or calcium ionophore (109).

An important aspect to consider in defining the role of mitochondria in the process of apoptosis is the anti-apoptotic proto-oncogene bcl-2, which encodes a protein localized in the outer mitochondrial membrane as well as endoplasmic reticulum and nuclear membrane (56, 97). Overexpression of Bcl-2 has been previously shown to suppress lipid peroxidation and ROS generation as well as prevent mitochondrial uncoupling (44, 50, 127). The Bcl-2 localization studies suggest that Bcl-2 may function directly at the mitochondrial membranes in these effects (42). Bcl-2 is not detectable in Colo-205 cells by Western blot (Mancini, M., and B. Anderson, unpublished result), but other members of this family may function as survival factors in Colo-205 cells. In addition to decreased expression or inhibitory posttranslational modifications, the protective effect of Bcl-2–like proteins could be diluted out by increased mitochondrial mass. Alternatively, Bcl-2 function might be restricted to specific mitochondrial subsets.

Finally, the relationship between mitochondrial proliferation and cell cycle arrest may be important. Mitochondrial proliferation is associated with cell cycle arrest in G_2/M in Colo-205 cells after herbimycin treatment. Cell cycle arrests in *Saccharomyces cerevisiae* and *Schizosaccharomyces pombe* are associated with continued mitochondrial replication, eventually leading to abnormal mitochondrial morphologies (78, 104). Mitochondrial proliferation may be a manifestation of continued cell growth dissociated from cell cycle regulation (58). Dissociation between cytoplasmic and nuclear cell cycle events has been described in CHO cells after treatment with multiple cytostatic agents (59). In this model, a linear relationship between increased cellular size after exposure to the drug and decreased viability has been shown. G_2 may be a sensitive phase of the cell cycle for dissociation of cytoplasmic and nuclear events in Colo-205 cells.

In conclusion, herbimycin A induces a proliferation of dysfunctional mitochondria together with enterocytic differentiation in Colo-205 cells. These mitochondrial changes are preceded by cell cycle arrest and followed by apoptosis. The association of cell cycle arrest, mitochondrial abnormalities, and apoptosis may be a useful model to explain the linkage of terminal differentiation to apoptosis in numerous cell lineages.

The authors are indebted to Andrew Berger for his excellent technical assistance in flow cytometry experiments and analysis of cell cycle data; to Judy Groombridge for the preparation of electron microscopy specimens; and to Paul Goodman, Paula Salewsky, and Tim Knight for their assistance with computer graphics and image analysis. We are grateful to Michael Wright and Stephen Schwartz for providing the rat liver nuclei preparation for in vitro assays of apoptosis.

D.M. Hockenberry is a Lucille P. Markey scholar, and this work was supported by a grant from the Lucille P. Markey Charitable Trust.

Received for publication 11 July 1996 and in revised form 5 May 1997.

References

1. Arends, M.J., R.G. Morris, and A.H. Wyllie. 1990. Apoptosis. The role of the endonuclease. *Am. J. Path.* 136:593–608.
2. Arnaudo, E., M.C. Dalakas, S. Shanske, C. Moraes, S. Di Mauro, and E. Schon. 1991. Depletion of muscle mitochondrial DNA in AIDS patients with Zivudine-induced myopathy. *Lancet.* 337:508–510.
3. Aruoma, O.I., B. Halliwell, B.M Hoey, and J. Butler. 1989. The antioxidant action of N-acetyl cysteine: its reaction with hydrogen peroxide, hydroxyl radical, superoxide and hypoclorous acid. *Free Radical Biol. Med.* 6:593–597.
4. Attardi, G., and G. Schatz. 1988. Biogenesis of mitochondria. *Annu. Rev. Cell Biol.* 4:289–333.
5. Bass, D.A., J.W. Parce, L.R. Dechatelet, P. Szejda, M.C. Seeds, and M. Thomas. 1983. Flow cytometric studies of oxidative products formulation by neutrophils: a graded response to membrane stimulation. *J. Immunol.* 130:1910–1917.
6. Beere, H.M., and J.A. Hickman. 1993. Differentiation: a suitable strategy for cancer chemotherapy? *Anti-Cancer Drug Des.* 8:299–322.
7. Bernardi, P., K.M. Broekemeier, and D.R. Pfeiffer. 1994. Recent progress on regulation of the mitochondrial permeability transition pore; a cyclosporine-sensitive pore in the inner mitochondrial membrane. *J. Bioenerg. Biomembr.* 26:509–516.
8. Boise, L.H. 1993. Bcl-X, a bcl-2 related gene that functions as a dominant regulator of apoptotic cell death. *Cell.* 74:597–608.
9. Boveris, A., and B. Chance. 1973. The mitochondrial generation of hydrogen peroxide. *Biochem. J.* 134:707–716.
10. Burton, K. 1956. A study of the conditions and mechanism of the diphenylamine reaction for the colorimetric estimation of deoxyribonucleic acid. *Biochem. J.* 62:315–323.
11. Busciglio, J., and B.A. Jankner. 1995. Apoptosis and increased generation of reactive oxygen species in Down's syndrome neurons *in vitro. Nature (Lond.).* 378:776–779.
12. Buttke, T.M., and P.A. Sandstrom. 1994. Oxidative stress as a mediator of apoptosis. *Immunol. Today.* 15:7–10.
13. Carbonari, M., M. Cibati, M. Cherchi, D. Sbarigia, A.M. Pesce, L. Dell'Anna, A. Modica, and M. Fiorilli. 1994. Detection and characterization of apoptotic peripheral blood lymphocytes in human immunodeficiency virus infection and cancer chemotherapy by a novel flow immunocytometric method. *Blood.* 83:1268–1277.
14. Chen, L.B., I.C. Summerhayes, L.V. Johnson, M.L. Walsh, S.D. Bernal, and T.J. Lampidis. 1981. Probing mitochondrial living cells with rhodamine 123. *Cold Spring Harbor Symp. Quant. Biol.* 46:141–155.
15. Cheng, H., and C.P. Leblond. 1974. Origin, differentiation and renewal of the four main epithelial cell types in the mouse small intestine. I–V. *Am. J. Anat.* 141:461–562.
16. Chomienne, C., P. Ballerini, M. Huang, M. Cornic, J.P. Abita, S. Castaigne, and L. Degos. 1990. In vitro effect of retinoic acid. *Nouv. Rev. Fr. Hematol.* 32:32–34.
17. Counis, M.F., E. Chaudun, B. Allinquat, A.S. Muel, M. Sanwal, C. Skidmore, and Y. Courtis. 1989. The lens: a model for chromatin degradation studies in terminally differentiated cells. *Int. J. Biochem.* 21:235–242.
18. Crissaman, H.A., and G.T. Hirons. 1994. Staining of DNA in live and fixed cells. *In* Methods in Cells Biology. Second Edition. Vol. 41. Z. Darzynkiewicz, J.P. Robinson, and M.A. Crissaman, editors. Academic Press, Inc., San Diego. 195–210.
19. Cupler, E.J., M.J. Danon, C. Jay, K. Hench, M. Ropka, and M.C. Dalakas. 1995. Early features of zivudine-associated myopathy: histopathological findings and clinical correlations. *Acta Neuropathol.* 90:1–6.
20. Darzynkiewicz, Z., S. Bruno, G. Del Bino, W. Gorczyca, M.A. Hotz, P. Lassota, and F. Traganos. 1992. Features of apoptotic cells measured by flow cytometry. *Cytometry.* 13:795–808.
21. Darzynkiewicz, Z., X. Li, and J. Gong. 1994. Assays of cell viability: discrimination of cells dying by apoptosis. *In* Methods in Cells Biology. Second Edition. Vol. 41. Z. Darzynkiewicz, J.P. Robinson, and M.A. Crissaman, editors. Academic Press, Inc., San Diego. 15–38.

22. Degos, L., H. Dombret, C. Chomienne, M.T. Daniel, J.M. Micl'ea, C. Chastang, S. Castaigne, and P. Fenaux. 1995. All-*trans*-retinoic acid as a differentiating agent in the treatment of acute promyelocytic leukemia. *Blood.* 86:2643–2653.
23. Delia, D., A. Aiello, D. Soligo, E. Fontanell, C. Melani, F. Pezzella, M.A. Pierotti, and G. Della Porta. 1992. Bcl-2 proto-oncogene expression in normal and neoplastic human myeloid cells. *Blood.* 79:1291–1298.
24. Dunnen, R.D., and K. Ebisuzaki. 1992. The linking of anticancer drugs, cell cycle blocks, and differentiation: implications in the search for antineoplastic drugs. *Leuk. Res.* 16:491–495.
25. Enari, M., R.V. Talanian, W.W. Wong, and S. Nagata. 1996. Sequential activation of ICE-like and CPP32-like proteases during Fas-mediated apoptosis. *Nature (Lond.).* 380:723–726.
26. Fenaux, P., M.C. Le Deley, S. Castaigne, E. Archimbaud, C. Chomienne, H. Link, A. Guerci, M. Duarte, M.T. Daniel, D. Bowen, et al., 1993. Effect of all transretinoic acid in newly diagnosed acute promyelocytic leukemia. Results of a multicenter randomized trial. European APL 91 Group. *Blood.* 82:3241–3249.
27. Ferrari, S., A. Grande, R. Manfredini, and U. Torelli. 1992. Terminal differentiation. *Ann. NY Acad. Sci.* 663:180–186.
28. Fliedner, T.M., E.P. Cronkite, and J.S. Robertson. 1964. Granulocytopoiesis. I. Senescence and random loss of neutrophilic granulocytes in human beings. *Blood.* 24:402–414.
29. Froelich, C.J., K. Orth, J. Turbov, P. Seth, R. Gottlieb, B. Babior, G.M. Shah, R.C. Bleackley, V.M. Dixit, and W. Hanna. 1996. New paradigm for lymphocyte granule-mediated cytotoxicity. *J. Biol. Chem.* 271: 29073–29079.
30. Gansler, H., and C. Rouiller. 1956. Modifications physiologiques et pathologiques du chondriome. Etude au microscope electronique. *Schweiz. Z. Allg. Pathol. Bacteriol.* 1956:217–243.
31. Garden, G.A., K.S. Canady, D.I. Lurie, M. Bothwell, and E.W. Rubel. 1994. A biphasic change in ribosomal conformation during transneuronal degeneration is altered by inhibition of mitochondrial, but not cytoplasmic protein synthesis. *J. Neurosci.* 14:1994–2008.
32. Gavrieli, Y., Y. Sherman, and S.A. Ben-Sasson. 1992. Identification of programmed cell death in situ via specific labeling of nuclear DNA fragmentation. *J. Cell Biol.* 119:493–501.
33. Ghadially, F.N. 1988. Ultrastructural Pathology of the Cell and Matrix. Third Edition. Butterworths, London.
34. Gorczyca, W., J. Gong, and Z. Darzynkiewicz. 1993. Detection of DNA strand breaks in individual apoptotic cells by the *in situ* terminal deoxynucleotidyl transferase and nick translation assays. *Cancer Res.* 53: 1945–1951.
35. Hackenbrock, C.R. 1968. Chemical and physical fixation of isolated mitochondria in low-energy and high-energy states. *Proc. Natl. Acad. Sci. USA.* 61:598–605.
36. Hackenbrock, C.R. 1968. Ultrastructural bases for metabolically linked mechanical activity in mitochondria. *J.Cell Biol.* 37:345–369.
37. Hackenbrock, C.R., T.G. Rehn, E.C. Weinbach, and J.J. Lemasters. 1971. Oxidative phosphorylation and ultrastructural transformation in mitochondria in the intact ascites tumor cell. *J. Cell Biol.* 51:123–131.
38. Harmon, B., L. Bell, and L. Williams. 1984. An ultrastructural study of the "meconium corpuscles" in rat foetal intestinal epithelium with particular reference to apoptosis. *Anat. Embryol (Berl.).* 169:119–124.
39. Heerdt, B.G., and L.H. Augenlicht. 1991. Effects of fatty acids on expression of genes encoding subunits of cytochrome c oxidase and cytochrome c oxidase activity in HT29 human colon adenocarcinoma cells. *J. Biol. Chem.* 266:19120–19126.
40. Heerdt, B.G., M.A. Houston, J.J. Rediske, and L.H. Augenlicht. 1996. Steady-state levels of mitochondrial messenger RNA species characterize a predominant pathway culminating in apoptosis and shedding of HT29 human colonic carcinoma cells. *Cell Growth Differ.* 7:101–106.
41. Henkart, P.A., and S. Grinstein. 1996. Apoptosis: mitochondria resurrected? *J. Exp. Med.* 183:1293–1295.
42. Hockenbery, D., G. Nuñez, C. Milliman, R.D. Schreiber, and S.J. Korsmeyer. 1990. Bcl-2 is an inner mitochondrial membrane protein that blocks programmed cell death. *Nature (Lond.).* 348:334–336.
43. Hockenbery, D., M. Zutter, W. Hickey, M. Nahm, and S.J. Korsmeyer. 1991. Bcl-2 protein is topographically restricted in tissues characterized by apoptotic cell death. *Proc. Natl. Acad. Sci. USA.* 88:6961–6965.
44. Hockenbery, D.M., Z.N. Oltvai, X. Yin, C.L. Milliman, and S.J. Korsmeyer. 1993. Bcl-2 functions in an antioxidant pathway to prevent apoptosis. *Cell.* 75:241–251.
45. Honma, Y., J. Okabe-Kado, M. Hozumi, Y. Uehara, and S. Mizuno. 1989. Induction of erythroid differentiation of K562 human leukemic cells by herbimycin A, an inhibitor of tyrosine kinase activity. *Cancer Res.* 49: 331–334.
46. Hunter, D.R., and R.A. Haworth. 1979. The Ca^{2+}-induced membrane transition in mitochondria. III. Transitional Ca^{2+} release. *Arch. Biochem. Biophys.* 195:468–477.
47. Hyde, G.E., and D. Durham. 1994. Rapid increase in mitochondrial volume in nucleus magnocellularis neurons following cochlea removal. *J. Comp. Neurol.* 339:27–48.
48. James, T.N., F. Terasaki, E.R. Pavlovich, and A.M. Vikhert. 1993. Apoptosis and pleomorphic micromitochondriosis in the sinus nodes surgically excised from five patients with the long QT syndrome. *J. Lab. Clin. Med.* 122:309–323.
49. Johnson, L.V., M.L. Walsh, and L.B. Chen. 1980. Localization of mitochondria in living cells with rhodamine 123. *Proc. Natl. Acad. Sci. USA.* 77:990–994.
50. Kane, D.J., T.A. Serafian, T.A. Anton, H. Hahn, E.B. Gralla, J.S. Valentine, T. Ord, and D.E. Bredesen. 1993. Bcl-2 inhibition of neuronal death: decreased generation of reactive oxygen species. *Science (Wash. DC).* 262:1274–1277.
51. Kaufmann, S.H., S. Desnoyers, Y. Ottaviano, N. Davidson, and G.G. Poirier. 1993. Specific proteolytic cleavage of poly(ADP-ribose) polymerase: an early marker of chemotherapy-induced apoptosis. *Cancer Res.* 53:3976–3985.
52. Kerr, J.F.R. 1971. Shrinkage necrosis: a distinct mode of cellular death. *J. Pathol.* 105:13–20.
53. Kerr, J.F.R., A.H. Wyllie, and A.R. Currie. 1972. Apoptosis: a basic biological phenomenon with wide-ranging implications in tissue kinetics. *Br. J. Cancer.* 26:239–257.
54. Kluck, R.M., E. Bossi-Wetzel, D.R. Green, and D. Newmeyer. 1997. The release of cytochrome c from mitochondria: a primary site for Bcl-2 regulation of apoptosis. *Science (Wash. DC).* 275:1132–1136.
55. Kozopas, K.M., T. Yang, H.L. Buchan, P. Zhou, and R.W. Craig. 1993. MCL-1, a gene expressed in programmed myeloid differentiation, has sequence similarity to Bcl-2. *Proc. Natl. Acad. Sci. USA.* 90:3516–3520.
56. Krajewski, S., S. Tanaka, S. Takayama, M.J. Schibler, W. Fenton, and J.C. Reed. 1993. Investigation of the subcellular distribution of the Bcl-2 oncoprotein: residence in the nuclear envelope, endoplasmic reticulum, and outer mitochondrial membrane. *Cancer Res.* 53:4701–4714.
57. Kroemer, G., N. Zamzami, and S.A. Susin. 1996. Mitochondrial control of apoptosis. *Immunol. Today.* 18:44–51.
58. Kung, A.L., A. Zetterberg, S.W. Sherwood, and R.T. Schimke. 1990. Cytotoxic effects of cell cycle phase specific agents: results of cell cycle perturbation. *Cancer Res.* 50:7307–7317.
59. Kung, A.L., S.W. Sherwood, and R.T. Schimke. 1993. Differences in the regulation of protein synthesis, cyclin B accumulation, and cellular growth in response to the inhibition of DNA synthesis in Chinese Hamster Ovary and HeLa S3 cells. *J. Biol. Chem.* 268:23072–23080.
60. Laiho, K.U., and B.F. Trump. 1975. Studies on the pathogenesis of cell injury. Effect of inhibitors of metabolism and membrane function on the mitochondria of Erlich ascites tumor cells. *Lab. Invest.* 32:163–182.
61. Laiho, K.U., J.D. Shelburne, and B.F. Trump. 1971. Observations on cell volume, ultrastructure, mitochondrial conformation, and vital-dye uptake in Erlich ascites tumor cells. *Am. J. Pathol.* 65:203–229.
62. Lazebnik, Y.A., S. Cole, C.A. Cooke, W.G. Nelson, and W.C. Earnshaw. 1993. Nuclear events of apoptosis in vitro in cell-free mitotic extracts: a model system for analysis of the active phase of apoptosis. *J. Cell Biol.* 123:7–22.
63. Lazebnik, Y.A., S.H. Kaufman, S. Desnoyers, G.G. Poirer, and W.C. Earnshaw. 1994. Cleavage of poly(ADP-ribose) polymerase by a proteinase with properties like ICE. *Nature (Lond.).* 371:346–347.
64. Li, X., F. Traganos, M.R. Melamed, and Z. Darzynkiewicz. 1995. Single-step procedure for labeling DNA strand breaks with fluorescein- or BODIPY-conjugated deoxynucleotides: detection of apoptosis and bromodeoxyuridine incorporation. *Cytometry.* 20:172–180.
65. Liu, X., C.N. Kim, J. Yang, R. Jemmerson, and X. Wang. 1996. Induction of apoptotic program in cell-free extracts: requirement for dATP and cytochrome C. *Cell.* 86:147–157.
66. Lu, Q.L., R. Poulson, L. Wong, and A.M. Hanby. 1993. Bcl-2 expression in adult and embryonic non-hematopoietic tissues. *J. Pathol.* 169:431–437.
67. Maftah, A., J.M. Petit, M.H. Ratinaud, and R. Julien. 1989. 10-N nonylacridine orange: a fluorescent probe which stains mitochondria independently of their energetic state. *Biochem. Biophys. Res. Commun.* 164:185–190.
68. Majno, G., and I. Joris. 1995. Apoptosis, oncosis, and necrosis. An overview of cell death. *Am. J. Pathol.* 146:3–15.
69. Mannweiler, K., and W. Bernhard. 1957. Recherches ultrastructurales sur une tumeur renale experimentale du hamster. *J. Ultrastruct. Res.* 1:158–169.
70. Marchetti, P., S.A. Susin, D. Decaudin, S. Gamen, M. Castedo, T. Hirsch, N. Zamzami, J. Naval, A. Senik, and G. Kroemer. 1996. Apoptosis-associated derangement of mitochondrial function in cells lacking mitochondrial DNA. *Cancer Res.* 56:2033–2038.
71. Martin, S.J., D.D. Newmeyer, S. Mathias, D.M. Farschon, H.G. Wang, J.C. Reed, R.N. Kolesnick, and D.R. Green. 1995. Cell-free reconstitution of Fas-, UV radiation-, and ceramide-induced apoptosis. *EMBO (Eur. Mol. Biol. Organ.) J.* 14:5191–5200.
72. Matsukawa, Y., N. Marui, T. Sakai, Y. Satomi, M. Yoshida, K. Matsumoto, H. Nishino, and A. Aoike. 1993. Genistein arrests cell cycle progression at G_2-M. *Cancer Res.* 53:1328–1331.
73. Mayer, M., and M. Noble. 1994. N-Acetyl-L-cysteine is a pluripotent protector against cell death and enhancer of trophic factor-mediated cell survival *in vitro. Proc. Natl. Acad. Sci. USA.* 91:7496–7500.
74. Meister, A., and M. Anderson. 1983. Glutathione. *Annu. Rev. Biochem.* 52:711–760.

75. Modica-Napolitano, J.S. 1993. AZT causes tissue-specific inhibition of mitochondrial bioenergetic function. *Biochem. Biophys. Res. Commun.* 194:170–177.
76. Murukami, Y., S. Mizuno, M. Hori, and Y. Uehara. 1988. Reversal of transformed phenotypes by herbimycin A in *src* oncogene expressed rat fibroblasts. *Cancer Res.* 48:1587–1590.
77. Neutra, M.R. 1988. The gastrointestinal tract. *In* Cell and Tissue Biology. A Textbook of Histology. L. Weiss, editor. Urban and Schwarzenberg, Baltimore, MD. 643–683.
78. Newlon, C.S., and W.L. Fangman. 1975. Mitochondrial DNA synthesis in cell cycle mutants of *Saccharomyces cerevisiae. Cell.* 5:423–428.
79. Newmeyer, D.D., D.M. Farschon, and J.C. Reed. 1994. Cell-free apoptosis in *Xenopus* egg extracts: inhibition by Bcl-2 and requirement for an organelle fraction enriched in mitochondria. *Cell.* 79:353–364.
80. Nicholls, D.G., and R.M. Locke. 1984. Thermogenic mechanisms in brown fat. *Physiol. Rev.* 64:1–64.
81. Nicholson, W.D., A. Ali, N.A. Thornberry, J.P. Vaillancourt, C.K. Ding, M. Gallant, D.K. Miller, et al., 1995. Identification and inhibition of the ICE/CED-3 protease necessary for mammalian apoptosis. *Nature (Lond.).* 376:37–43.
82. Nicoletti, I., G. Migliorati, M.C. Pagliacci, F. Grignani, and C. Riccardi. 1991. A rapid and simple method for measuring thymocyte apoptosis by propidium iodide staining and flow cytometry. *J. Immunol. Methods.* 139:271–276.
83. Ohashi, H., A. Ichikawa, H. Takagi, T. Hotta, T. Naoe, R. Ohno, and H. Saito. 1992. Remission induction of acute promyelocytic leukemia by all-*trans*-retinoic acid: molecular evidence of restoration of normal hematopoiesis after differentiation and subsequent extinction of leukemic clone. *Leukemia (Baltimore).* 6:859–862.
84. Omura, S., Y. Iwai, Y. Takahashi, N. Sadakane, and A. Nakagawa. 1979. Herbimycin, a new antibiotic produced by a strain of *Streptomyces. J. Antibiot.* 32:255–261.
85. Papadimitriou, J.C., C.B. Drachenberg, M.L. Shin, and B.F. Trump. 1994. Ultrastructural studies of complement mediated cell death: a biological reaction model to plasma membrane injury. *Virchows Arch.* 424:677–685.
86. Peled-Kamar, M., J. Lotem, E. Okon, L. Sachs, and Y. Groner. 1995. Thymic abnormalities and enhanced apoptosis of thymocytes and bone marrow cells in transgenic mice overexpressing Cu/Zn-superoxide dismutase: implications for Down syndrome. *EMBO (Eur. Mol. Biol. Organ.) J.* 14:4985–4993.
87. Petit, P.X., J.E. O'Connor, D. Grunwald, and S.C. Brown. 1990. Analysis of the membrane potential of rat- and mouse-liver mitochondria by flow cytometry and possible applications. *Eur. J. Biochem.* 194:389–397.
88. Petit, J.M., A. Maftah, M.H. Retinaud, and R. Julien. 1992. 10-N nonyl acridine orange interacts with cardiolipin and allows the quantification of this phospholipid in isolated mitochondria. *Eur. J. Biochem.* 209:267–273.
89. Petit, P.X., H. Lecoeur, E. Zorn, C. Dauguet, B. Mignotte, and M.-L. Gougeon. 1995. Alterations in mitochondrial structure and function are early events of dexamethasone-induced thymocyte apoptosis. *J. Cell Biol.* 130:157–167.
90. Potten, C.S., and T.D. Allen. 1977. Ultrastructure of cell loss in intestinal mucosa. *J. Ultrastruct. Res.* 60:272–277.
91. Raff, M.C. 1992. Social controls on cell survival and cell death. *Nature (Lond.).* 356:397–400.
92. Rapoport, S.M., T. Schewe, R. Wiesner, W. Halangk, P. Ludwig, M. Janicke-Hohne, C. Tannert, C. Hiebsch, and D. Klatt. 1979. The lypoxygenase of reticulocytes. Purification, characterization and biological dynamics of the lipoxygenase; its identity with the respiratory inhibitors of the reticulocyte. *Eur. J. Biochem.* 96:545–561.
93. Reed, J.R. 1994. Bcl-2 and the regulation of programmed cell death. *J. Cell. Biol.* 124:1–6.
94. Reers, M., T.W. Smith, and L.B. Chen. 1991. J-aggregate formation of a carbocyanine as a quantitative fluorescent indicator of membrane potential. *Biochemistry.* 30:4480–4486.
95. Reipert, S., J. Berry, M.F. Hughes, J.A. Hickman, and T.D. Allen. 1995. Changes of mitochondrial mass in the hemopoietic stem cell line FDCP-mix after treatment with etoposide: a correlative study by multiparameter flow cytometry and confocal and electron microscopy. *Exp. Cell Res.* 221:281–288.
96. Ricquier, D., L. Casteilla, and F. Bouillaud. 1991. Molecular studies of the uncoupling protein. *FASEB (Fed. Am. Soc. Exp. Biol.) J.* 5:2237–2249.
97. Riparbelli, M.G., G. Callaini, S.A. Tripodi, M. Cintorino, P. Tosi, and R. Dallai. 1995. Localization of the Bcl-2 protein to the outer mitochondrial membrane by electron microscopy. *Exp. Cell Res.* 221:363–369.
98. Roche, S., S. Fumagalli, and S.A. Courtneidge. 1995. Requirement for Src family protein tyrosine kinases in G_2 for fibroblast cell division. *Science (Wash. DC).* 269:1567–1569.
99. Rothe, G., and G. Valet. 1990. Flow cytometric analysis of respiratory burst activity in phagocytes with Hydroethidine and 2′,7′–dichlorofluorescin. *J. Leukocyte Biol.* 47:440–448.
100. Rouiller, C. 1957. Contribution de la microscopie electronique a l'etude du foie normal et pathologique. *Ann. Anat. Pathol.* 2:548–562.
101. Rouiller, C., and G. Simon. 1962. Contribution de la microscopie electronique au progres de nos connaissances en cytologie et en histo-pathologie hepatique. *Rev. Internat. Hepat.* 12:167–206.
102. Rubel, E.W., R.L. Hyson, and D. Durham. 1990. Afferent regulation of neurons in the brain stem auditory system. *J. Neurobiol.* 21:169–196.
103. Saunders, J.W., and J.F. Fallon. 1967. Cell death in morphogenesis. *In* Problems in Developmental Biology. Academic Press, New York. 289–314.
104. Sazer, S., and S.W. Sherwood. 1990. Mitochondrial growth and DNA synthesis occur in the absence of nuclear DNA replication in fission yeast. *J. Cell Sci.* 97:509–516.
105. Schewe, T., S.P.J. Albracht, and P. Ludwig. 1981. On the site of action of the inhibition of the mitochondrial respiratory chain by lipoxygenase. *Biochim. Biophys. Acta.* 636:210–217.
106. Schlegel, J., I. Peters, S. Orrenious., D.K. Miller, N.A. Thornberry, T.T. Yamin, and D.W. Nicholson. 1995. CPP32/Apopain is a key interleukin 1β converting enzyme-like protease involved in Fas-mediated apoptosis. *J. Biol. Chem.* 271:1841–1844.
107. Searle, J., T.A. Lawson, P.J. Abbott, B. Harmon, and J.F. Kerr. 1975. An electron-microscope study of the mode of cell death induced by cancer-chemotherapeutic agents in populations of proliferating normal and neoplastic cells. *J. Pathol.* 116:129–138.
108. Semple, T.I., L.A. Quinn, L.K. Woods, and G.E. Moore. 1978. Tumor and lymphoid cell lines from a patient with carcinoma of the colon for a cytotoxicity model. *Cancer Res.* 38:1345–1355.
109. Shimizu, S., Y. Eguchi, W. Kamiike, S. Waguri, Y. Uchiyama, H. Matsuda, and Y. Tsujimoto. 1996. Bcl-2 blocks loss of mitochondrial membrane potential while ICE inhibitors act at a different step during inhibition of death induced by respiratory chain inhibitors. *Oncogene.* 13:21–29.
110. Simpson, M.V., C.D. Chin, S.A. Keilbough, T.S. Lin, and W.H. Prusoff. 1989. Studies on the inhibition of mitochondrial DNA replication of 3′-azido-3′-deoxythymidine and other dideoxynucleoside analogs which inhibit HIV-1 replication. *Biochem. Pharmacol.* 38:1033–1036.
111. Smiley, S.T., M. Reers, C. Mottola-Hartson, M. Lin, A. Chen, T.W. Smith, G.D. Steele, Jr., and L. Chen. 1991. Intracellular heterogeneity in mitochondrial membrane potentials revealed by a J-aggregate-forming lipophilic cation JC-1. *Proc. Natl. Acad. Sci. USA.* 88:3671–3675.
112. Smith, M.A., D.R. Parkinson, B.D. Cheson, and M.A. Friedman. 1992. Retinoids in cancer therapy. *J. Clin. Oncol.* 10:839–864.
113. Staal, F.J., M. Roederer, L.A. Herzenberg, and L.A. Herzenberg. 1990. Intracellular thiols regulate activation of nuclear factor *K*B and transcription of human immunodeficiency virus. *Proc. Natl. Acad. Sci. USA.* 87:9943–9947.
114. Svoboda, D.J., and J. Higginson. 1963. Ultrastructural hepatic changes in rats on a necrogenic diet. *Am. J. Pathol.* 43:477–495.
115. Tewari, M., L. Quan, K. O'Rourke, S. Desnoyers, Z. Zeng, D.R. Beidler, G.G. Poirier, G.S. Salvesen, and V.M. Dixit. 1995. Yama/CPP32β, a mammalian homolog of ced-3, is a CrmA-inhibitable protease that cleaves the death substrate poly(ADP-ribose) polymerase. *Cell.* 81:801–809.
116. Tidball, J.G., D.E. Albrecht, B.E. Lokensgard, and M.J. Spencer. 1995. Apoptosis precedes necrosis of dystrophin-deficient muscle. *J. Cell. Sci.* 108:2197–2204.
117. Turrens, J.F., and A. Boveris. 1980. Generation of superoxide anion by the NADH dehydrogenase of bovine heart mitochondria. *Biochem. J.* 191:421–427.
118. Uehara, Y., M. Hori, T. Tackeuchi, and H. Umezawa. 1985. Screening of agents which convert 'transformed morphology' of Rous sarcoma virus-infected rat kidney cells to 'normal morphology': identification of an active agent as herbimycin and its inhibition of intracellular *src* kinase. *Jpn. J. Cancer Res.* 76:672–675.
119. Uehara, Y., M. Hori, T. Takeuchi, and H. Umezawa. 1986. Phenotypic change from transformed to normal induced by benzoquinonoid ansamycins accompanies inactivation of $p60^{src}$ in rat kidney cells infected with Rous sarcoma virus. *Mol. Cell. Biol.* 6:2198–2206.
120. Uehara, Y., Y. Murukami, S. Mizuno, and S. Kawai. 1988. Inhibition of transforming activity of tyrosine kinase oncogenes by herbimycin A. *Virology.* 164:294–298.
121. Uehara, Y., H. Fukazawa, Y. Murakami, and S. Mizuno. 1989. Irreversible inhibition of v-src tyrosine kinase activity by herbimycin A and its abrogation by sulfhydryl compounds. *Biochem. Biophys. Res. Commun.* 163:803–809.
122. Uehara, Y., Y. Murakami, Y. Sugimoto, and S. Mizuno. 1989. Mechanism of reversion of Rous sarcoma virus transformation by herbimycin A: reduction of total phosphotyrosine levels due to reduced kinase activity and increased turnover of p60vsrc-1. *Cancer Res.* 49:780–785.
123. Vayssiere, J.L., P.X. Petit, Y. Risler, and B. Mignotte. 1994. Commitment to apoptosis is associated with changes in mitochondrial biogenesis and activity in cell lines conditionally immortalized with simian virus 40. *Proc. Natl. Acad. Sci. USA.* 91:11752–11756.
124. Wachstein, M., and M. Besen. 1964. Electron microscopy of renal coagulative necrosis due to dl-serine, with special reference to mitochondrial pyknosis. *Am. J. Pathol.* 44:383–400.
125. Weedon, D., J. Searle, and J.F.R. Kerr. 1979. Apoptosis. Its nature and implications for dermatopathology. *Am. J. Dermatopathol.* 1:133–144.

126. Wyllie, A.H. 1992. Apoptosis and the regulation of cell number in normal and neoplastic tissues: an overview. *Cancer Metastasis Rev.* 1:95–103.
127. Zamzami, N., P. Marchetti, M. Castedo, D. Decaudin, A. Macho, T. Hirsch, S.A. Susin, P.X. Petit, B. Mignotte, and G. Kroemer. 1995. Sequential reduction of mitochondrial transmembrane potential and generation of reactive oxygen species in early programmed cell death. *J. Exp. Med.* 182:367–377.
128. Zamzami, N., S.A. Susin, P. Marchetti, T. Hirsch, I. Gomez-Monterrey, M. Castedo, and G. Kroemer. 1996. Mitochondrial control of nuclear apoptosis. *J. Exp. Med.* 183:1533–1544.
129. Zoratti, M., and I. Szabo. 1994. Electrophysiology of the inner mitochondrial membrane. *J. Bioenerg. Biomembr.* 26:543–553.
130. Zucchetti, M., C.V. Catapano, S. Filippeschi, E. Erba, and M. D'Incalci. 1989. Temozolomide induced differentiation of K562 leukemia cells is not mediated by gene hypomethylation. *Biochem. Pharmacol.* 38:2069–2075.